Indian Journal of Engineering & Materials Sciences
Vol. 31, December 2024, pp. 864-887
DOI: 10.56042/ijems.v31i6.8771

Design of multiband miniaturized MIMO antenna with defected ground for future mobile communications

Gudi Guru Prasad* & Gopal Senthil Kumar

Sri Chandrasekharendra Saraswathi Viswa Mahavidyalaya, Kanchipuram, Tamil Nadu 631 561, India

Received: 13 February 2024; accepted: 26 October 2024

A multiband four port 4 element slotted 2x2 MIMO antenna for future mobile communication is presented in this paper. The proposed antenna consists of a modified square slot at the center of the patch and eighteen rectangular slots around the borders of the patch in the form of a modified Sierpinski carpet fractal structure. Miniaturization and multiband characteristics have been obtained with the help of a novel modified fractal structure. Then two such antennas have been combined to form a 2x1 MIMO antenna. Further 2x2 MIMO antenna has been designed with 4 elements. The proposed 2x2 MIMO antenna consists of four novel modified Sierpinski carpet-shaped antenna elements. Four antenna elements have been closely separated with $\lambda/2$. Novel defected ground structures with ellipses have been made to achieve high isolation within 4-elements of the MIMO antenna. The designed antenna has been simulated for different combinations of Active sources and phase shifts. The designed antenna has been fabricated, and the results have been measured. The diversity parameter such as ECC < 0.001, ensures that the proposed design is suitable for the MIMO applications. The novel design structure enhanced multiband characteristics and improved miniaturization represent that the proposed antenna will be an efficient candidate for future wireless communication systems including IoT and Biomedical applications.

Keyword*:* Defected ground, Future mobile communications, Miniaturized, Multi-band, Sierpinski carpet fractal structure

1 Introduction

Present MIMO systems, there will be interaction between antennas. This interaction changes the current distribution and input impedance of normal independent antennas. Space allocated for the antenna on mobile is less due to the requirement for smartphone size to be small. Hence the spacing between antenna elements of a MIMO antenna have been reduced which results in mutual coupling effect and reduces antenna performance. A lot of research is going on to address this effect by researchers nowadays and provide certain solutions with some advantages and disadvantages. Normally microstrip antennas have limitations like single frequency operation, lower gain, larger size, and polarization issues. For enhancing the limitations of conventional patch antennas, several techniques are used like stacked structures, frequency-selected surfaces, feeding with different techniques, metamaterials, defected grounds, and Electromagnetic band gaps. The defected ground technique is a popular one among the different techniques listed above due to its simplicity.

Making some defects or slots on a ground plate of the patch antenna is referred to as defected ground. Defected ground may contain single or multiple defects. The earlier defected ground concept is used under microstrip lines to stop unwanted frequencies and reduce mutual coupling between elements. Normally DGS were made in microstrip antennas to improve the gain and reduces the higher directive harmonics, mutual coupling and improve radiation properties of patch antenna. EBG technology means having periodical defected shapes on the ground to suppress surface currents, hence improving the efficiency of antenna and gain. slots of special geometry were made on the defected part on ground. These slots can be periodic or a periodic. Any defect that is made on the ground plane disturbs in current distributions on the ground and alters some characteristics including slot inductance, slot resistance, and the slot capacitance that alter the operating bands of frequency.

Equivalent circuit model for DGS: The conductive part of the microstrip antenna is the combinations of resistance, inductance, and capacitance. Babinates states that a slot will be reciprocal to the metallic structure. Hence, represented by equivalent resistance, inductance, and capacitance models. Previously there were some trial-and-error iteration methods that were used but they are time-consuming processes, and they

*Corresponding author (E-mail: guru.p6@gmail.com)

were unpopular. Different equivalent circuits of DGS are.

(i) RLC and LC equivalent circuits
(ii) Π shaped equivalent circuits
(iii) Quasi-state equivalent circuits
(iv) Using an ideal transformer

The slotted part of DGS is directly proportionate to effective inductance and contrariwise proportional to the effective capacitance. Thus, increasing or declining the DGS area will result in changing the operating frequency. Increasing the slot area will reduce resonant frequency and reducing DGS area reduces effective capacitances and increases the resonant frequency. Reactance (X_{LC}) of lowpass Butterworth filter is

$$X_{LC} = 1/\ \omega_0 C\ (\omega_0/\omega - \omega/\ \omega_0) \quad \ldots(1)$$

where ω_0 is angular resonant frequency, f_0 is resonant frequency, $L= 1/4\pi f_0^2 C$ and $C= \omega_c/Z_0 g_i * 1/(\omega_0^2 - \omega_c^2)$

DGS for Circular polarization: Present wireless communication devices require circularly polarized antennas for applications in mobile communications, WLANs, GPS systems, and RFID readers. DGS is employed on the ground plate of antenna to achieve circular polarization. Multiband and wideband antennas can also be achieved by using defective grounds.

Miniaturization of Antenna using DGS: Effective inductance and capacitance changes by employing slots on the ground resulting in shifting the resonant frequency to the lower side. Hence, miniaturization was achieved with the help of DGS. Some slots of different geometry were embedded on the ground to achieve antenna miniaturization.

Cross-polarization reduction using DGS: DGS can be used to suppress cross-polarization in the radiation of the antenna. It can be achieved by using dot-shaped or arc-shaped DGS.

Envelope correlation coefficient (ECC) is given by

$$\varrho e = \frac{|s11s12+s21s22|}{(1-|s11|2-|s21|)(1-|s22|-|s12|)} \quad \ldots(2)$$

ECC represents how two antenna radiation patterns are independent. For MIMO, ECC must be < (0.3-0.4)

Researchers applied different slotting techniques on patch and ground for MIMO antennas to achieve multi-band characteristics and reduce mutual coupling & improve isolation. Kin-Lu Wong, et al. designed Eight eight-port angular ring slotted patches with 16 shorting pins connected to a circular grounded MIMO antenna designed for mobiles. From circular patches, 8 angular ring patches are made with the help of 8 open slots. Each angular ring patch is fed with a probe feed technique to form 8 ports. Below to feed point, towards the center 2 shorting pins were used to short patches and ground to suppress standing waves and hence improve the isolation between patches. So low value of ECC < 0.1 is achieved for MIMO operation. The designed antenna operated at 5.9- 7.2 GHz in the 6GHz band which can be used for future 6G mobile communications and IoT[1]. MD. Abu Sufian et.al designed four square-shaped patches, placed in an orthogonal manner on the substrate. Circular-shaped parasites were incorporated between 4 square patches to reduce mutual coupling effect between nearby antenna elements. Designed antenna operated at 5.82-5.94 GHz band with 7.68dBi gain. The decoupling structure consists of seven circular slots around a circular slot with four cuts in a crossed manner. The ground plane is defected with four arm fan-shaped defects to reduce mutual coupling effect between four adjacent square patches. The proposed antenna can be implemented for vehicles for intercommunication[2].

Sanjukta Nej, et al. designed Ten elements asymmetric U-shaped patch antenna on the Fr4 substrate to operate in the N258 band. An Elliptical-shaped slot is made at each patch area and an asymmetric U-shaped patch is inserted with the help of a coplanar waveguide. Here 10 ports were used to connect 10 asymmetric U patches. Defected ground with an elliptical shape is done to reduce mutual coupling connecting antennas. Selecting the shape and position of DGS plays a vital role in reducing surface currents and in turn minimizes mutual coupling effect and improves isolation[3]. Praveen Kumar, et al. designed a six-port symmetrical pyramid antenna using a novel defected ground plane with better isolation is presented in this paper. Rectangular-shaped defects were made on the ground bottom at each pyramid patch. This slot creates a disturbance in the current distribution and improves isolation. Two vertical branches and one horizontal branch were made on the ground to separate six grounds below six patches. Decoupling structure made on the ground creates reverse currents in opposite direction and minimize mutual coupling between elements[4].

Peng Fei Hu, et al. designed A miniaturized dual-band loop antenna to function at 2.4 GHz & 5 GHz WIFI bands. The circular loop antenna is fed with four strips connected to the center using a coaxial probe feed technique. Two loop patches are arranged compactly on a common substrate to operate at the 2.4GHz band and 5GHz band independently. A normal loop is used for the 2.4GHz band and the

Alford loop is used for the 5GHz band. Current if in phase, exhibits omnidirectional radiation pattern. Current if out of phase, resulting in cancellation of radiation fields in the azimuthal direction. Hence results in the splitting of the radiation pattern giving larger ripples. To solve this problem, one method used is by using an array of circular loops. The second method is by inserting parasitic strips in between adjacent elements. The third method is by using two radiators of omnidirectional pattern with different resonant frequencies and using LPF between two radiators to filter higher order modes[5]. Kin-Lu Wong, Hsuan-Jui, et al. Chang designed a Three port Y-shaped monopolar MIMO antenna, operating at 3.3-4.2 GHz. Three shorting strips were used at the three edges of Y and one strip on the center of Y was made to form three monopolar patches. A circular-shaped ground plate is used in the design with a coaxial probe feed technique. The designed antenna is used for 5G communication. The measured & simulated ECC for the proposed antenna is < 0.1 in the operated bands, which indicates better radiation characteristics of MIMO operation[6].

Jogesh Chandra Dash et al. designed Two closely spaced patches with an inverted L modeled structure connected at one end of each patch from top to bottom with rectangular DGS for 5G applications. Two patches are fed with a coaxial probe feeding technique. Inverted L-shaped structures were attached to patches to create asymmetry to reduce mutual coupling between patches and improve isolation[7]. JingYa Deng, JinYong Li., et al. designed A duo of symmetric inverted F-shaped patches on a common substrate. Ground is defected with the inverted T shape slot at the center position to achieve high isolation. For achieving broadband operation, two U-shaped slits were made on the feed line. The designed antenna is operated for WLAN applications in 2.4GHz and 5GHz bands. For feeding two antennas, the microstrip line feeding technique is used with an impedance of 50Ω. Generally, when more than two antennas are placed within space <ʎ/2, there will be a mutual coupling effect that degrades the radiation characteristics and channel capacity of the antenna. So, to avoid it, the defected ground, or DGS with slots on the feed line including additional decoupling structure. To achieve better impedance matching, slits of different geometries and positions were made on the feed line[8].

Wen Wang, Yongle Wu, et al. designed a circular patch antenna with two mirror symmetric L-shaped branches at two sides to function in dual bands of 5G. two such antennas were made on common ground to form MIMO. Between two antennas, a parasitic element of T shape is made so that it will introduce an inverse path to cancel mutual coupling and improve isolation. The lower resonant frequency is produced by a circular patch antenna and the upper resonant frequency is obtained by two L made branches. Two rectangular slots are made on the partial ground to alter the field circulation parameters in the communication line. Normally, gaps in the ground plane are made to change surface currents so that mutual link is reduced. T-shaped parasitic elements are introduced between antennas to improve isolation. By loading the decoupling structure, a strong current mainly concentrates on the antenna matched with the surface current on the ground so the current on ground is cut off, hence isolation is enhanced[9].

Zhuo-Lin Zhao, et al. designed an asymmetric coplanar strip dual band MIMO antenna for 5G communications. The two antenna elements are separated by a double-size Y structure, which is used to improve the isolation between ports. The double Y strip dimensions are varied on a trial-and-error basis to achieve high isolation. Each antenna consists of three types of rectangular patches with different slot dimensions and different angles of orientation to achieve two 5G bands i.e. (3.3-3.6 GHz) and (4.80- 5 GHz)[10]. The proposed antenna in ref[11] consists of 2 split ring cavity resonator which are fed by a C shaped strip line. 8 antennas were placed at four sides of the rectangle with a pair at each side. Between two patches, a rectangular slot is made to achieve isolation between ports. The dimensions of rectangular slots may be varied to achieve worthy isolation. When operating in the 2.6GHz band, the current distribution is in arm 1 and hence it is considered a folding monopole. If the current distribution in arms 1, and 2 at 2.95GHz, the current flows in the opposite direction resulting in a folding slot antenna. When surface current flowing in arm 3,4, is in the opposite direction at 4.85GHz, surface currents distribute on arm 4 only, and a folded monopole is realized. A 2-element inverted F MIMO antenna was designed to WLAN applications[12]. Two IFAs on top act as antenna 1, and 2, and the bottom layer with two angular slots acts as antenna 3, and 4. The two angular slots on the ground improve the isolation between elements. The novelty in this approach is converting the DGS structure on the ground to an

antenna. Two-element MIMO antenna is designed with each element containing two open L-shaped slots[13]. A narrow slot in the form of a diagonal is made on the ground to decrease mutual coupling between elements of the antenna. Sierpinski carpet-shaped Fractal with a modified antenna is designed with defected ground[17]. A multiband antenna is designed with a novel fractal shape and defected ground to function at different bands in wireless communication. Kaikai Song et al. designed dual-band printed monopole MIMO antenna to LTE and WLAN purposes[18]. However, the designed antenna can be operated at only two frequency bands. It was observed from the literature that every MIMO antenna design has its own advantages and disadvantages. Hence combining those techniques and including defected ground structures used in this proposed work to operate the antenna at Nine 5G NR bands including IoT, GPS, WIFI, and WIMAX frequency bands[19,20].

2 Materials and Methods

2.1 Geometry and analysis of proposed antenna

A modified Sierpinski carpet fractal slotted patch antenna using an Elliptical defected ground is designed for future mobile communication as shown in Fig. 1(a). It consists of 18 slots of similar geometry and dimensions that were made on the patch for multiband operation. Sierpinski carpet fractal slot is created on the center of the patch to compensate for the current dispersal on the patch and notch the unwanted frequency bands. Further 2x1 MIMO antenna is designed, displayed in Fig. 1(b). Two ports P1 and P2 were used to feed two antennas independently using the microstrip feeding technique. This combination of MIMO antenna may not improve throughput but decreases the block error rate. Further 2x2 MIMO antenna is designed for better throughput and gain as shown in Fig. 1(c). Fig. 1(d) shows the fabricated antenna.

The proposed antenna was designed using the popular substrate material FR4 (4.4) and thickness of 1.6mm. The total dimension of the proposed antenna is 57.8x76x1.6 mm^3. The structure of single antenna is shown in Fig.1. (a). The pink color portion represents the ground and white color represents the elliptical-shaped defected structure on the ground, eighteen equally placed slots around a modified dumbbell shape inside a rectangle represent patch. The structure of a 2x1 MIMO antenna representing two antenna elements is shown in Fig.1(b). The detailed structure of the 2x2 MIMO antenna representing four antennas is shown in Fig. 1(c). Microstrip feeding mechanisms were used for feeding the antenna elements. Dimensions of the antenna were optimized for operating the antenna at multiple required frequency bands. After finalizing the antenna structure, with the same dimensions, 2x1 MIMO and 2x2 MIMO

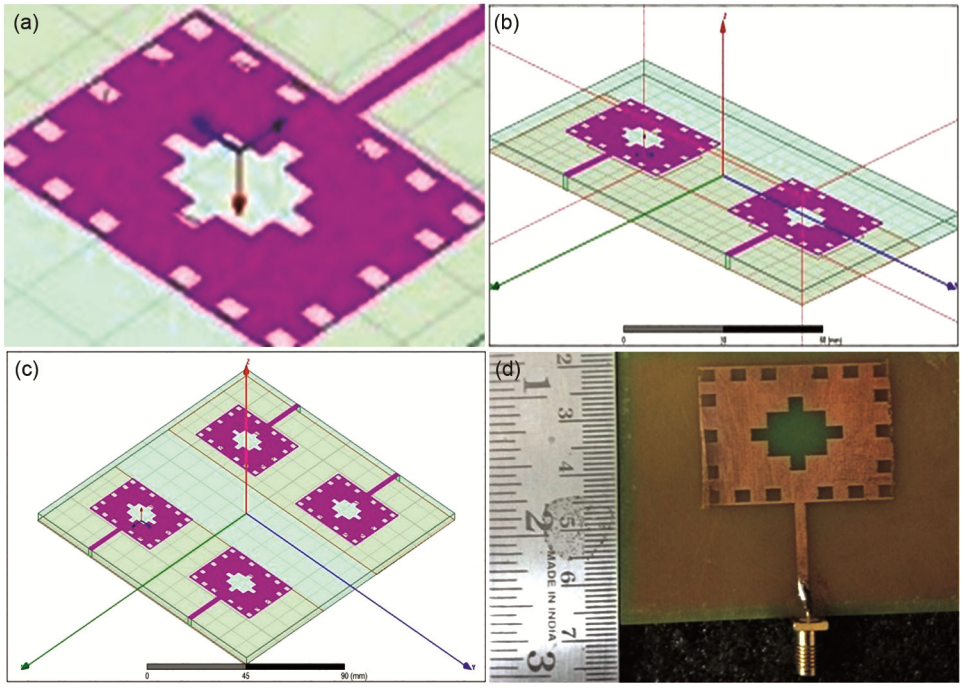

Fig. 1 — Geometry of the proposed Antenna (a) Geometry of single antenna with elliptical DGS, (b) Geometry of 2x1 MIMO antenna with elliptical DGS, (c) Geometry of 2x2 MIMO antenna with elliptical DGS, and (d) Fabricated Antenna.

antennas were developed. The defected ground technique is a popular method to improve isolation in MIMO. Here elliptical DGS is employed for better isolation. Based on the current distribution, the dimensions and spacing of slots are adjusted to improve separation between elements of antenna. In the second step for the 2x1 MIMO antenna, only one antenna is made active, and simulated results were measured. In the third step, two sources were made active and out of phase. Later both sources were made in phases. In the fifth step for the 2x2 MIMO antenna, one source is made active, and simulated results are measured. In the sixth step, opposite sources were made active and in phase. Later opposite sources are made active and out of phase. In eight steps, all sources were made active and in phase, and simulated results were measured later in the next step, all sources were made active and out of phase and simulated results were measured.

3 Results and Discussion

Multi-band antenna with single port, 2 port, and 4 ports were designed with different combinations of active sources and phase shifts. Simulated results of all cases were discussed in this section. Later, summary of the proposed antennas simulated & measured results were tabulated. Proposed antenna results were compared with other existing antenna designs and tabulated at the bottom of this section.

3.1 Simulated results for single antenna using elliptical DGS

3.1.1 Return loss

From the simulated plot, return loss for a single antenna using elliptical DGS is shown in Fig. 2(a), it is observed that the antenna is operated at 4 bands of frequency i.e. 1.5 GHz – 1.7 GHZ, 3.40GHz - 4.4GHz, 6.6GHz – 8.0GHz, 9.0GHz – 10.0GHz.

3.1.2 Measured return loss

From the measured plot, the return loss for a single antenna using elliptical DGS was shown in Fig.2(c). It is observed that the antenna is operated at 3 frequency bands i.e. 1.4 GHz –1.7 GHZ, 2.80GHz – 5.0GHz, 6.6GHz – 10GHz.

3.2 Simulated results for 2x1 MIMO antenna with elliptical DGS when one source is active

3.2.1 Return loss

S parameter of slotted 2x1 MIMO antenna using elliptical DGS when one source is active is noted in Fig. 3. It was observed that the antenna is operated at 4 bands i.e. 1.5 GHz– 1.80 GHz, 3.20GHz - 4.6GHz, 6.4GHz – 8.0GHz, 9.20GHz – 10 GHz.

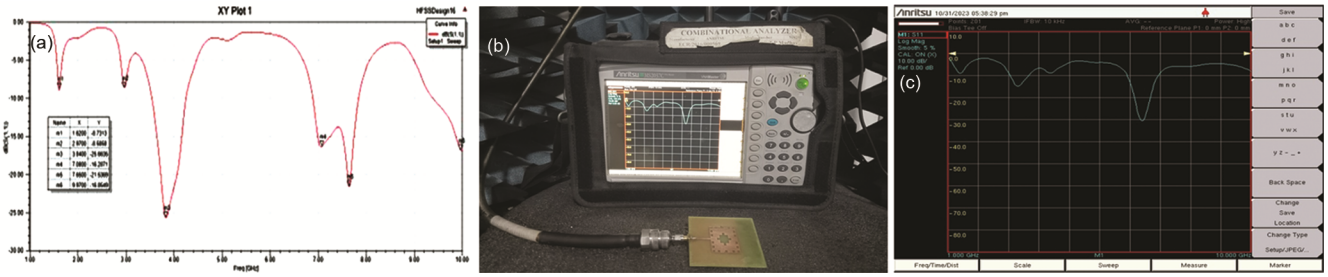

Fig. 2 — (a) Simulated S- parameter for single antenna with elliptical DGS, (b) Setup for Antenna Measurement and (c) Measured S- S-parameter for single antenna with elliptical DGS.

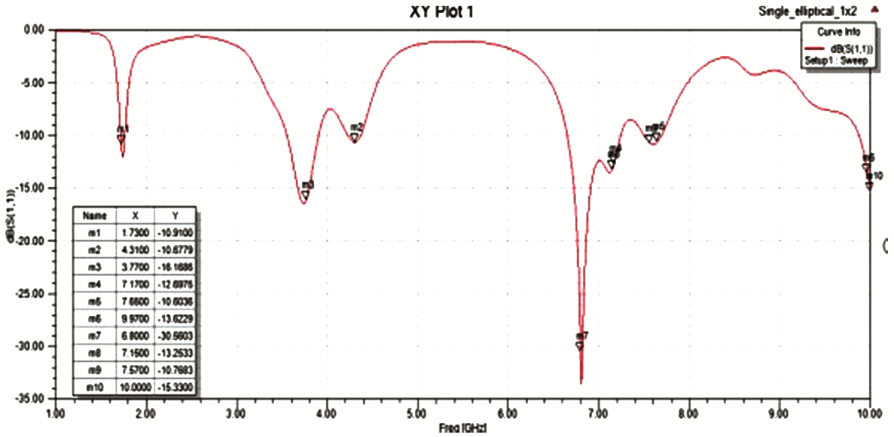

Fig. 3 — Simulated S parameter of 2x1 MIMO antenna with elliptical DGS when one source is active.

3.2.2 2D Radiation pattern

Figure 4 illustrates the simulated 2D radiation pattern of the 2x1 MIMO antenna with elliptical DGS when one source is active. Radiation patterns in principal planes were presented. Figure 4 (a), 4 (b) shows the 2D radiation pattern in 2 elevation planes, Θ= 360 X-Z plane, and pi= 360 Y-Z plane. Note that due to the symmetric shape in the antenna design, the radiation pattern was similar for all the combinations of antenna. Radiation patterns are similar of monopole were observed for which E_Θ field component represents a dip in broad side direction for $\Theta = 360^0$, $\Phi = 360^0$. the dip is shifted to 45^0 due to the presence of a symmetric structure. Epi component of $\Phi = 360^0$ is extended towards the broadside direction. Gain observed from the plot as 4.8dBi.

The simulated Gain of the 2x1 MIMO antenna using elliptical DGS when one source is active is displayed in Fig. 5. Observed Gain of the antenna is about 4.8dBi. The simulated Directivity of the 2x1 MIMO antenna with elliptical DGS when one source is active is denoted in Fig. 5. From the plot, it is noted that the Gain of the antenna is about 7.4dBi.

The radiation efficiency of an antenna is a measure of amount of power fed into the antenna input to the power radiated by an antenna.

3.2.3 Simulated results

Radiation Efficiency, Radiation Intensity, Radiated Power, and Beam Area of the Designed Antenna is shown in Fig. 6.

3.3 Simulated results for 2x1 MIMO antenna with elliptical DGS when two sources are active and in phase

Simulated results of the 2x1 MIMO antenna when two sources are active, and both are in phase were discussed here.

3.3.1 Return loss

The return loss of 2x1 MIMO antenna with elliptical DGS when one source is active is shown in

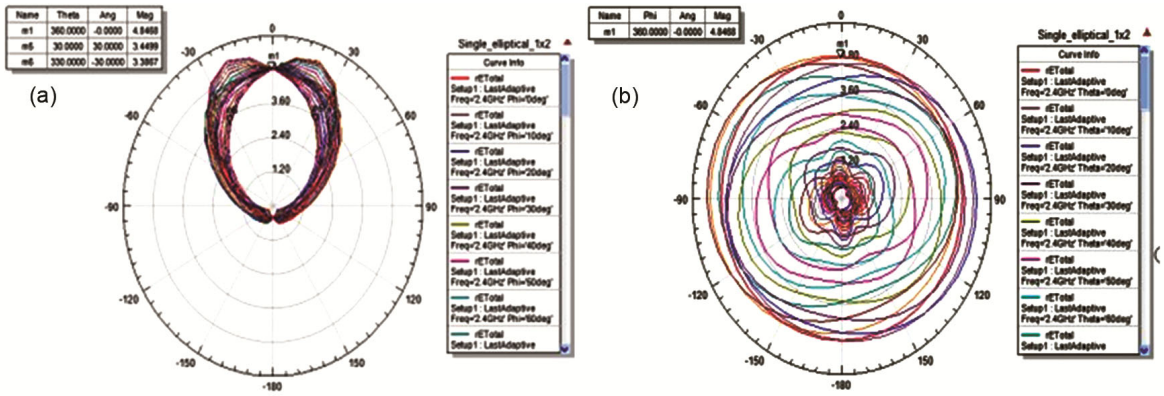

Fig. 4 — Simulated 2D Radiation pattern of 2x1 MIMO antenna using elliptical DGS: (a) for $\Theta = 360^0$ and (b) for $Pi = 360^0$.

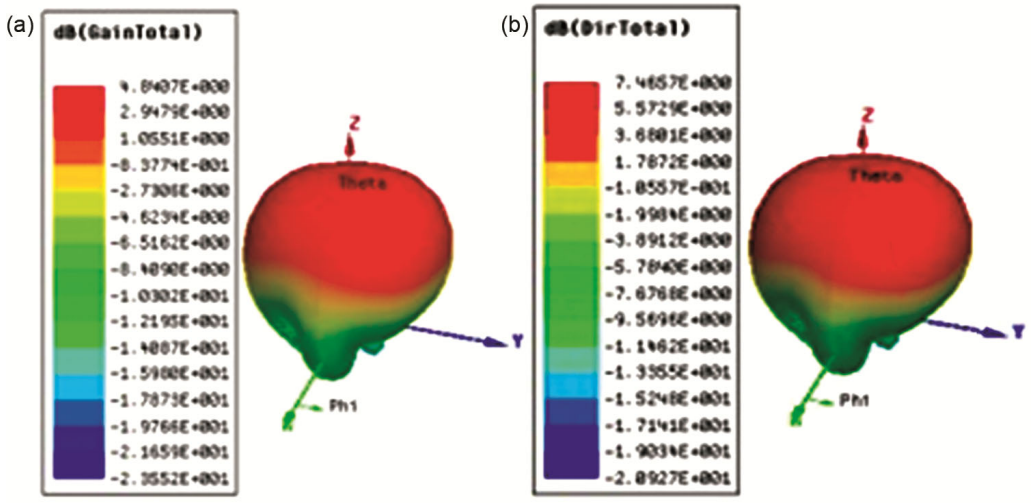

Fig. 5 — Simulated results of 2x1 MIMO antenna with elliptical DGS when one source is active (a) Gain, and (b) Directivity.

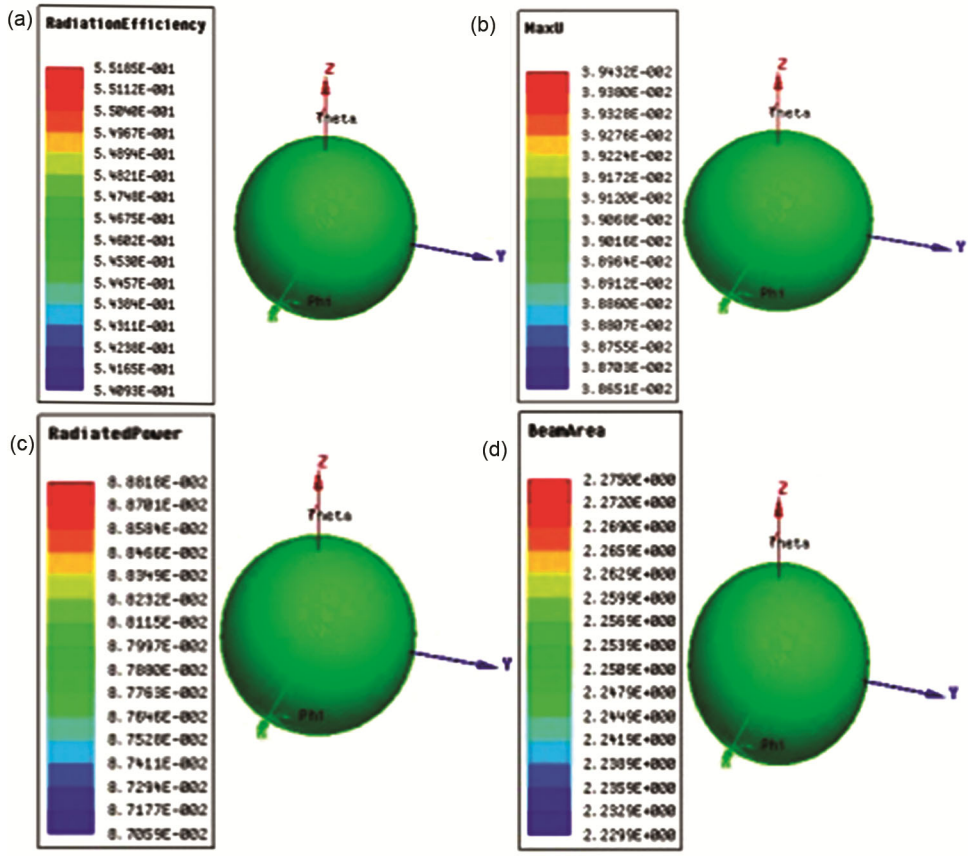

Fig. 6 — Simulated results of 2x1 MIMO antenna using elliptical DGS when one source is active (a) Radiation efficiency, (b) Radiation Intensity, (c) Radiated Power, and (d) Beam Area.

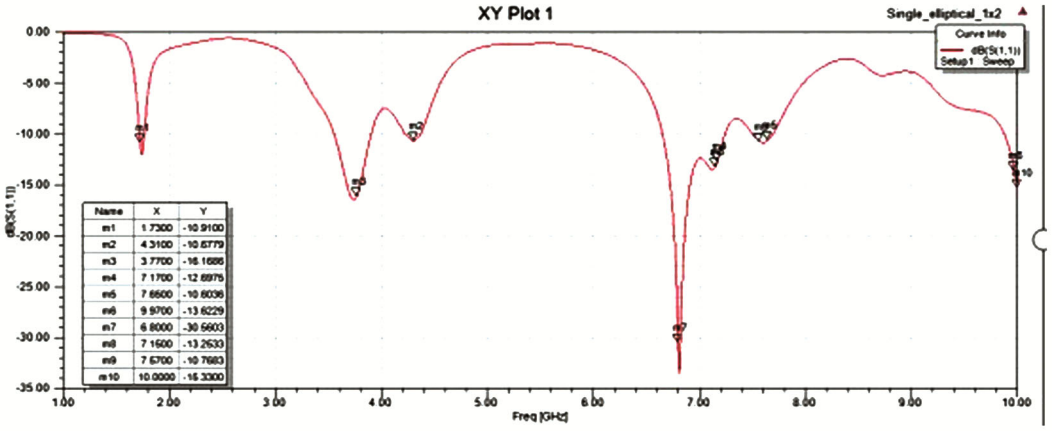

Fig. 7 — Simulated S-parameter of the 2x1 MIMO antenna with elliptical DGS for 2 sources active and in phase.

Fig. 7. And antenna functioned at 1.50 GHz – 1.80 GHZ, 3.2GHz - 4.6GHz, 6.4GHz – 8.0GHz, 9.20GHz - 10GHz bands.

3.3.2 2D Radiation pattern

Figure 8 directs the simulated 2D radiation pattern of the 2x1 MIMO antenna for 2 sources active and in phase. Radiation patterns in principal planes were presented. Figure 8 (a), 8 (b) directs the 2D radiation pattern in 2 elevation planes, Θ= 360 X-Z plane, and pi= 360 Y-Z plane. Radiation patterns similar of monopole were observed for which E_Θ field component represents a dip in broad side direction for $\Theta = 360^0$, $\Phi = 360^0$. the dip is shifted to 45^0 due to the presence of a symmetric structure. Epi component of $\Phi = 360^0$ is extended

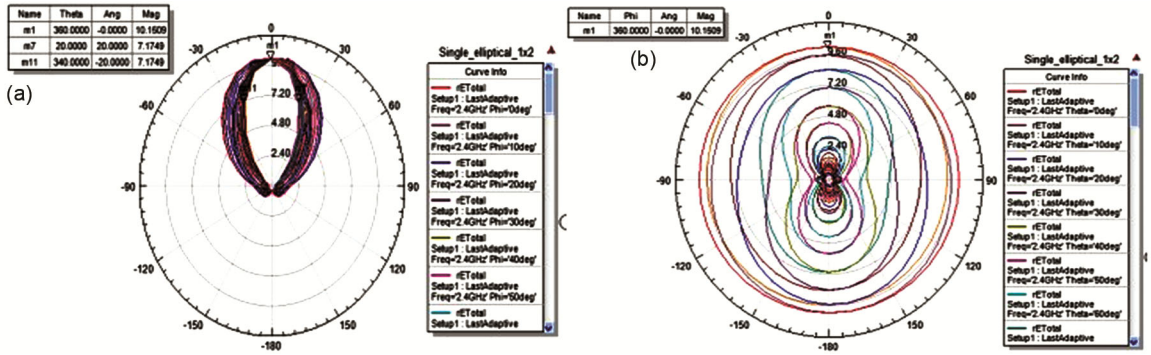

Fig. 8 — Simulated 2D Radiation pattern of 2x1 MIMO antenna with elliptical DGS for 2 sources active and in phase (a) for $\Theta = 360^0$, and (b) for $Pi = 360^0$.

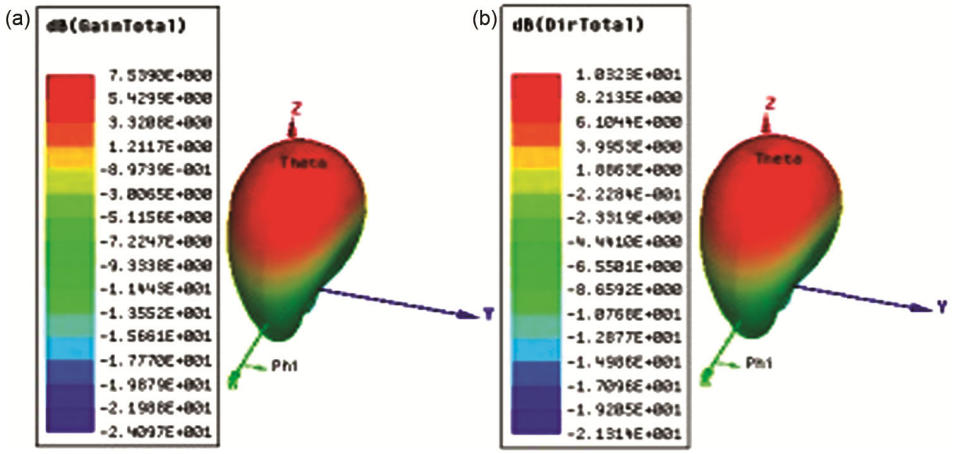

Fig. 9 — Simulated radiation patterns of the 2x1 MIMO antenna with elliptical DGS for 2 sources active and in phase (a) Gain, and (b) Directivity.

towards the broadside direction. Gain observed from the plot as 7.5dBi.

Simulated Gain of 2x1 MIMO antenna with elliptical DGS for 2 sources active and in phase is indicated in Fig. 9. Gain the of antenna observed is about 7.5dBi. The simulated Directivity of the 2x1 MIMO antenna for 2 sources active and in phase is illustrated in Fig. 9. From the plot, it is recorded that the Gain of the antenna is about 9.8dBi.

3.3.3 Simulated results

Radiation Efficiency, Radiation Intensity, Radiated Power, and Beam Area of the Designed Antenna is displayed in Fig. 10.

3.4 Simulated results for 2x1 MIMO antenna with elliptical DGS when two sources are active and out of phase

3.4.1 Return loss

The S parameter of the 2x1 MIMO antenna using elliptical DGS when one source is active is indicated in Fig. 11. Observed operated frequency bands are1.5 GHz – 1.80 GHZ, 3.2GHz - 4.6GHz, 6.4GHz – 8.0GHz, 9.20GHz - 10GHz.

The simulated Gain of 2x1 MIMO antenna with elliptical DGS when two sources are active and out of phase is illustrated in Fig. 12. The Gain of antenna observed is about 5.4dBi. The simulated Directivity of 2x1 MIMO antenna with elliptical DGS when one source is active is denoted in Fig. 12. The Directivity of the antenna observed is about 8.0dBi.

3.4.2 2D Radiation patterns

Figure 13 shows simulated 2D radiation pattern of 2x1 MIMO antenna for 2 sources active and out of phase. Radiation patterns in principal planes were presented. Figure 13 (a), 13 (b) indicates the 2D radiation pattern in 2 elevation planes, $\Theta = 360$ X-Z plane, and $pi = 360$ Y-Z plane. Radiation patterns similar of monopole were observed for which E_Θ field component represents a dip in end fire direction for $\Theta = 360^0$, $\Phi = 360^0$. the dip is shifted to 45^0 due to the presence of a symmetric structure. Epi component of $\Phi = 360^0$ is extended towards the broadside direction. Gain observed from the plot as 5.5dBi.

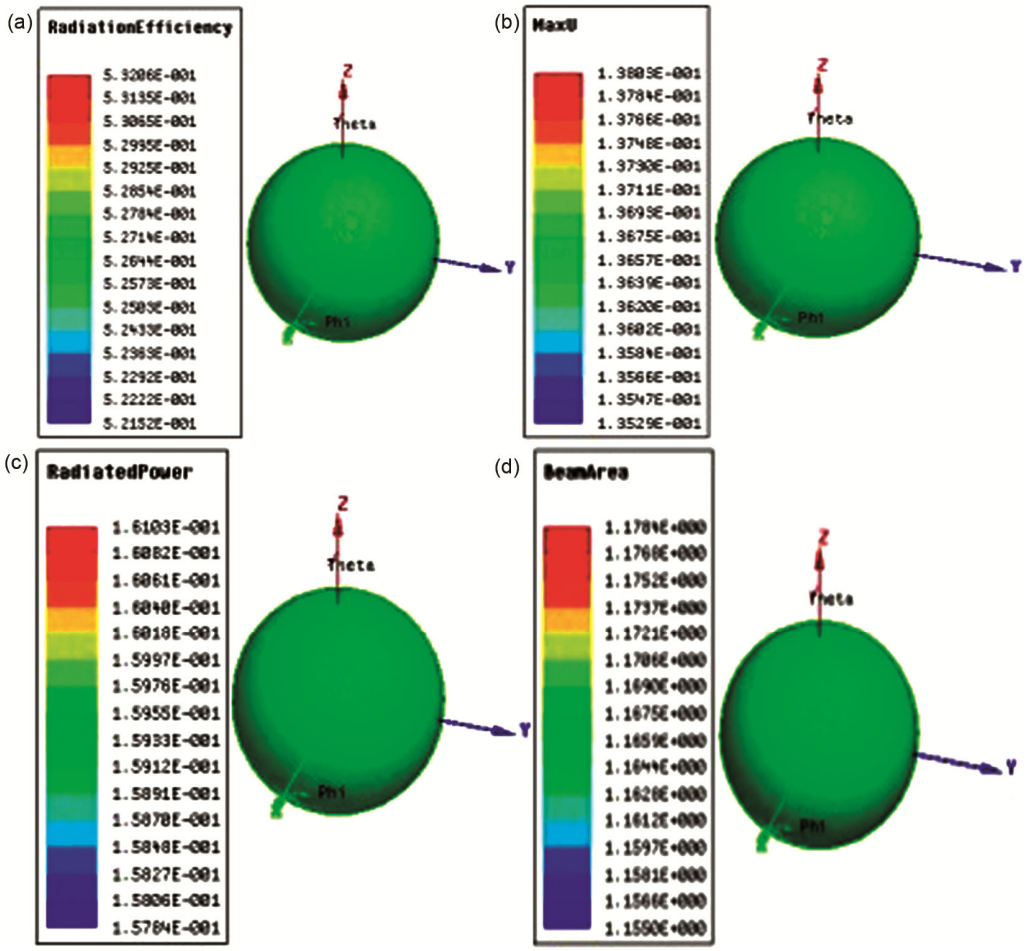

Fig.10 — Simulated results of the 2x1 MIMO antenna with elliptical DGS for 2 sources active and in phase (a) Radiation efficiency, (b) Radiation intensity, (c) Radiated power, and (d) Beam area.

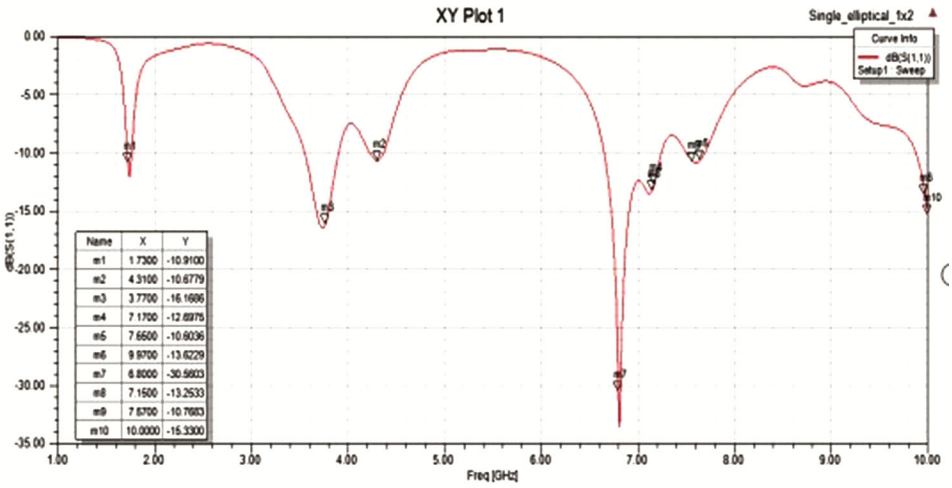

Fig. 11 — Simulated S-parameter of the 2x1 MIMO antenna with elliptical DGS for 2 sources active and out of phase.

3.4.3 Simulated results

Radiation Efficiency, Radiation Intensity, Radiated Power, and Beam Area of Designed Antenna is displayed in Fig. 14.

3.4.4 Envelope correlation coefficient (ECC)

Represents the correlation connecting antenna elements. It is calculated from the S-parameter or radiation pattern. Here ECC was calculated from the

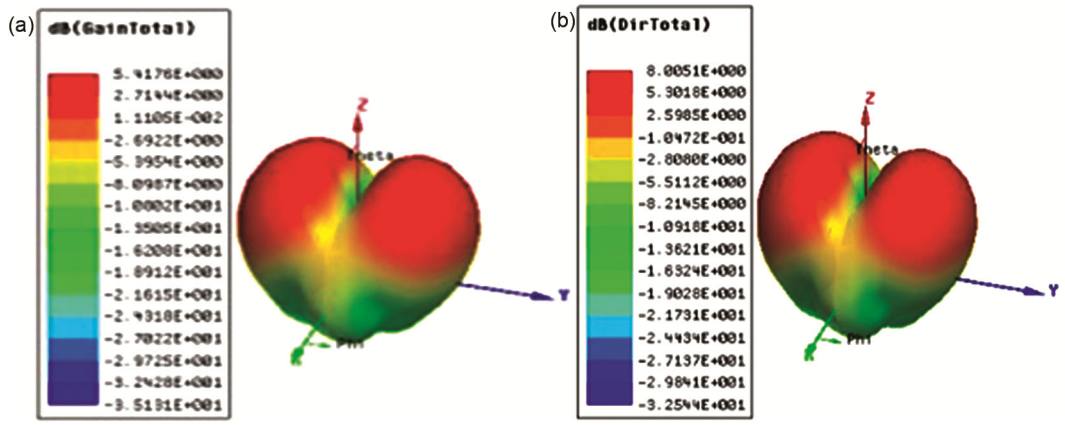

Fig. 12 — Simulated radiation patterns of 2x1 MIMO antenna with elliptical DGS for 2 sources active and out of phase (a) Gain, and (b) Directivity.

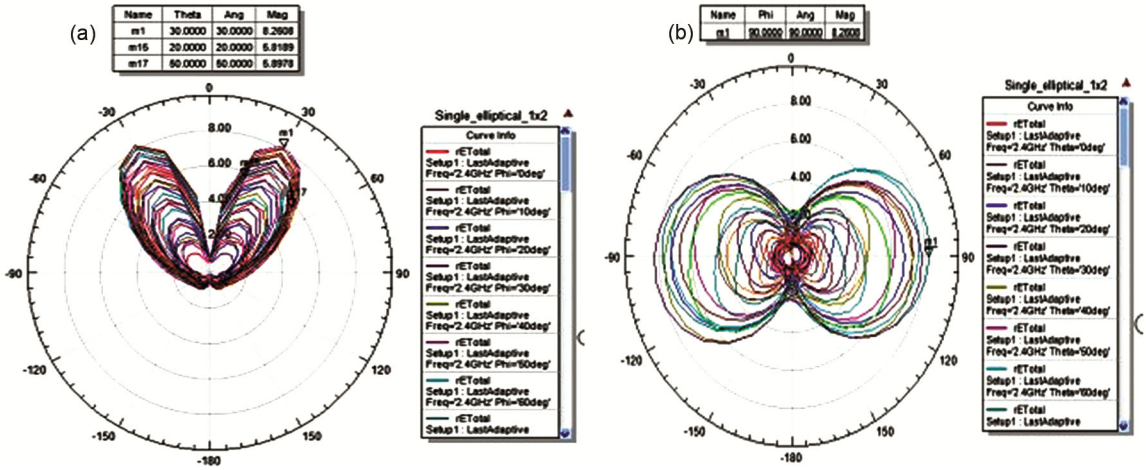

Fig. 13 — Simulated 2D Radiation pattern of 2x1 MIMO antenna with elliptical DGS for 2 sources active and out of phase: (a) for $\Theta = 360^0$, and (b) for $Pi = 360^0$.

S parameter as shown in Fig. 15. Normally ECC should be < 0.5 for MIMO antenna. From the simulated plot, ECC is less than 0.2 for all operating bands, which indicates that the designed MIMO antenna is appropriate for 5G with enhanced isolation.

3.5 Simulated results for 2x2 MIMO antenna with elliptical DGS when one source is active

3.5.1 Return loss

The return loss of 2x2 MIMO antenna with elliptical DGS when one source is active is shown in Fig. 16. From the plot, it is seen that the antenna functions at 4 bands i.e., 1.5 GHz – 1.80 GHZ, 3.2GHz - 4.6GHz, 6.4GHz – 8.0GHz, 9.20GHz – 10.0GHz.

3.5.2 2D Radiation patterns

Figure 17 displays the simulated 2D radiation patterns of 2x2 MIMO antenna for one source is active. Radiation patterns in principal planes were presented. Figure 17 (a), 17(b) shows the 2D radiation pattern in 2 elevated planes, $\Theta = 360$ X-Z plane, and $pi = 360$ Y-Z plane. Radiation patterns similar to monopole were observed for which E_Θ field component represents a dip in end fire direction for $\Theta = 360^0$, $\Phi = 360^0$. The dip is shifted to 60^0 due to the presence of a symmetric structure and a butterfly-like pattern is observed in Fig. 17. Epi component of $\Phi = 360^0$ is extended towards the broadside direction. Gain observed from the plot as 3.7dBi.

The simulated Gain of 2x2 MIMO antenna with elliptical DGS when one source is active is displayed in Fig. 18. The gain of the antenna is observed to be 3.7dBi. The simulated Directivity of 2x2 MIMO antenna with elliptical DGS when one source is active is denoted in Fig.18. The directivity of the antenna is observed as 6.8dBi.

3.5.3 Simulated results

Radiation Efficiency, Radiation Intensity, Radiated Power, and Beam Area of Designed Antenna is illustrated in Fig. 19.

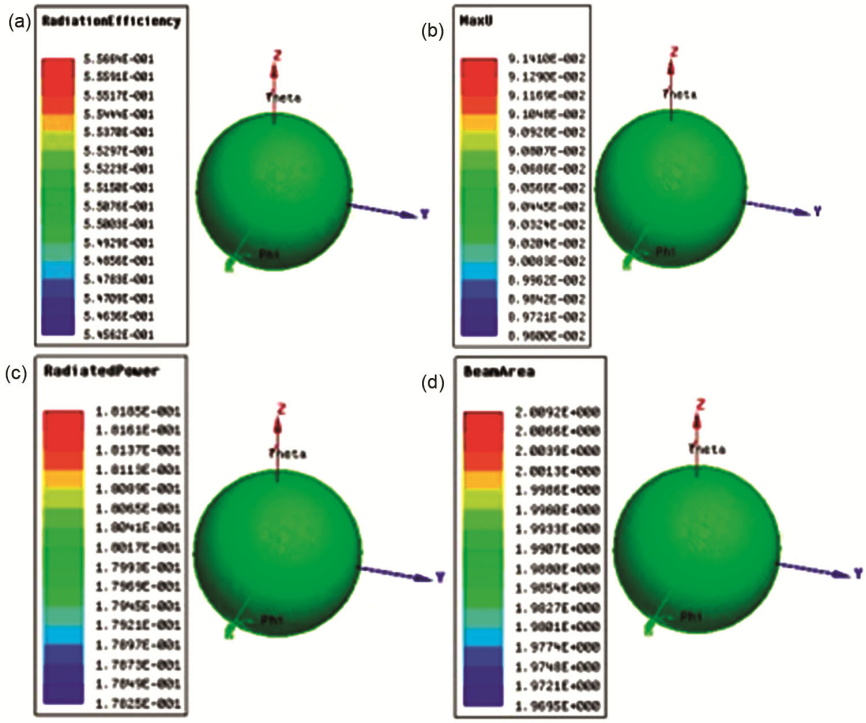

Fig. 14 — Simulated results of 2x1 MIMO antenna with elliptical DGS When both sources are active and out of phase (a) Radiation efficiency, (b) Radiation intensity, (c) Radiated power, and (d) Beam area.

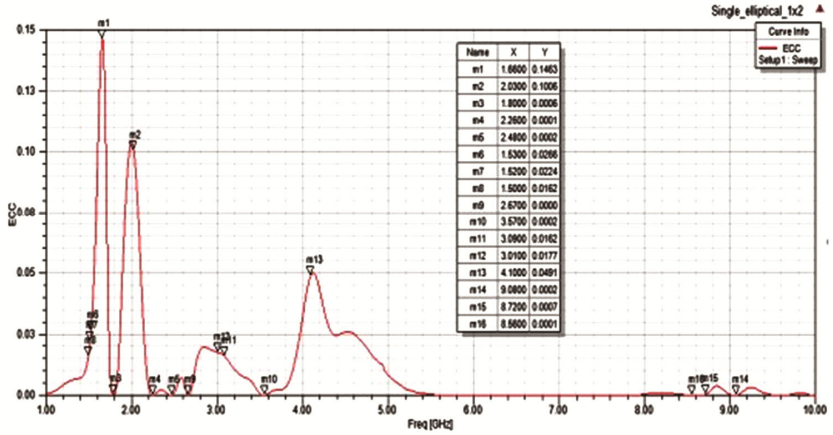

Fig. 15 — Simulated ECC of 2x1 MIMO antenna with elliptical DGS for 2 sources active and in-phase.

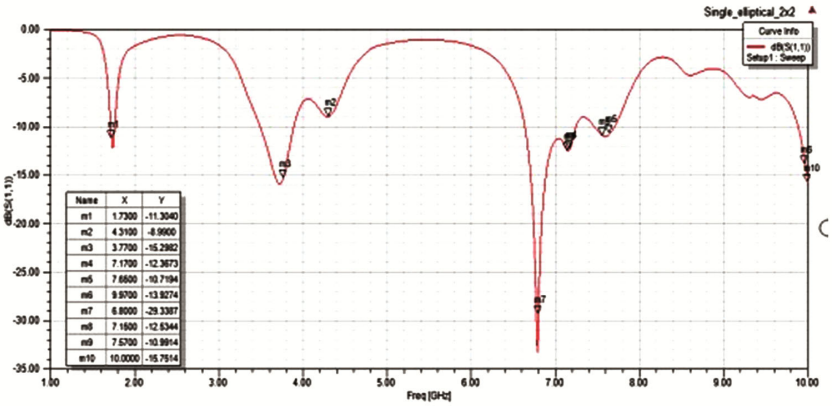

Fig. 16 — Simulated S-parameter of 2x2 MIMO antenna with elliptical DGS for one source active.

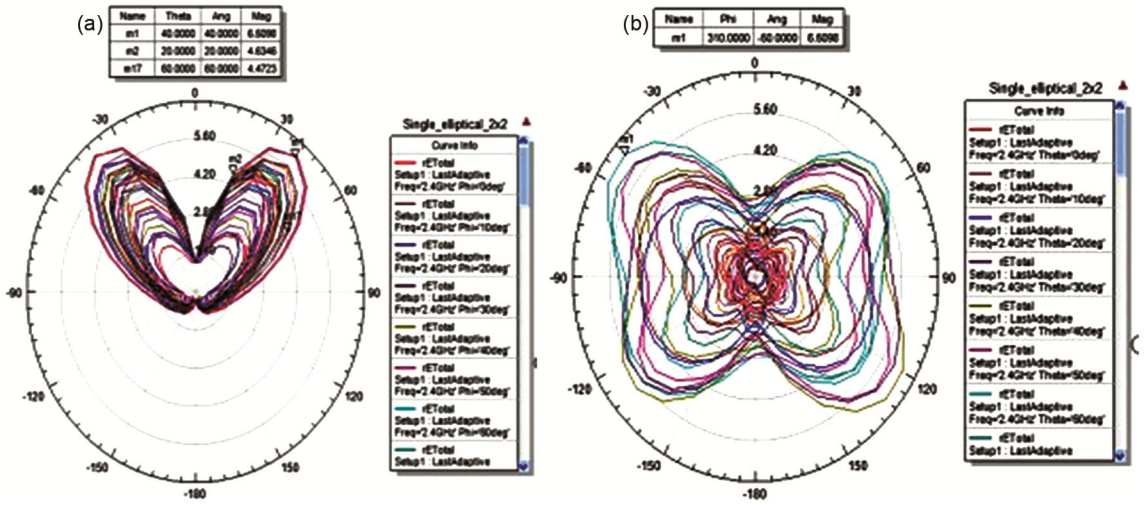

Fig. 17 — Simulated 2D radiation patterns of 2x2 MIMO antenna with elliptical DGS for one source active (a) for $\Theta = 360^0$, and (b) for $Pi = 360^0$.

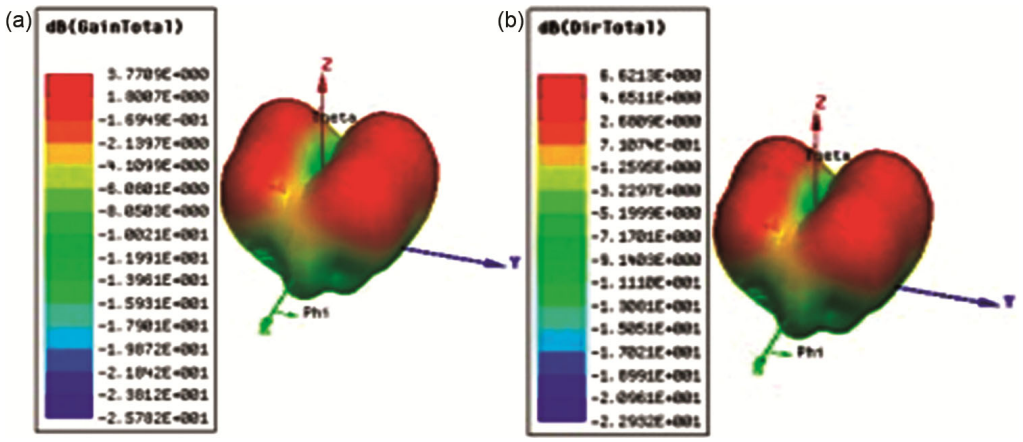

Fig. 18 — Simulated radiation pattern of 2x2 MIMO antenna with elliptical DGS for one source active (a) Gain, and (b) Directivity.

3.6 Simulated results for 2x2 MIMO antenna with elliptical DGS when opposite sources are active and in phase

3.6.1 Return loss

S parameter of the slotted antenna of 2x2 MIMO antenna with elliptical DGS when one source is active is shown in Fig. 20. From the plot, the antenna functions at 4 bands i.e. 1.50GHz – 1.80 GHZ, 3.2GHz - 4.6GHz, 6.4GHz – 8.0GHz, 9.20GHz - 10GHz.

3.6.2 2D Radiation patterns

Figure 21 shows simulated 2D radiation pattern of 2x2 MIMO antenna for opposite sources are active. Radiation patterns in principal planes were presented. Fig. 21(a), 21(b) exhibits the 2D radiation pattern in 2 elevation planes, Θ= 360 X-Z plane, and pi= 360 Y-Z plane. Radiation patterns similar of monopole were observed for which E_Θ field component represents a dip in end fire direction for $\Theta = 360^0$, $\Phi = 360^0$. The dip is shifted to 120^0 due to the presence of a symmetric structure. Epi component of $\Phi = 360^0$ is extended towards the end-fire direction. Gain observed from the plot as 6.2dBi.

The simulated Gain of 2x2 MIMO antenna with elliptical DGS when opposite sources are active is illustrated in Fig. 22. The Observed Gain of antenna is around 6.2dBi. The simulated Directivity of 2x2 MIMO antenna with elliptical DGS when one source is active is indicated in Fig. 22. The Directivity of antenna is 9.2dBi.

3.6.3 Simulated results

Radiation Efficiency, Radiation Intensity, Radiated Power, and Beam Area of Designed Antenna is shown in Fig. 23.

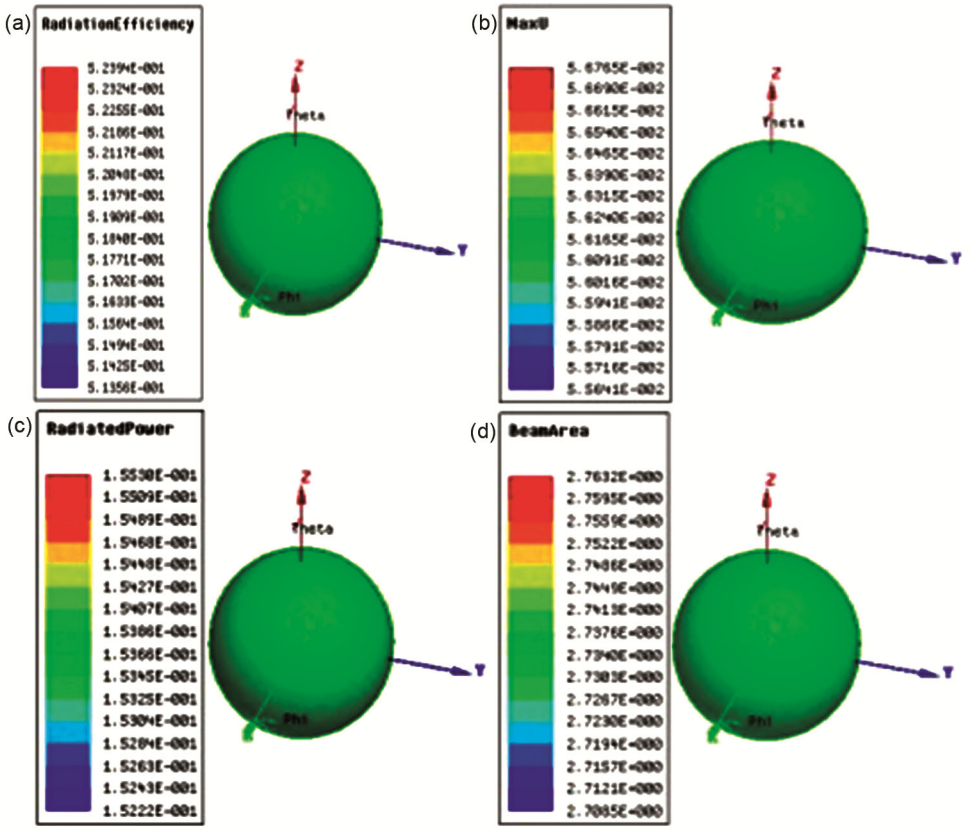

Fig. 19 — Simulated results of 2x2 MIMO antenna with elliptical DGS When one source is active a) Radiation efficiency, (b) Radiation intensity, (c) Radiated power, and (d) Beam area.

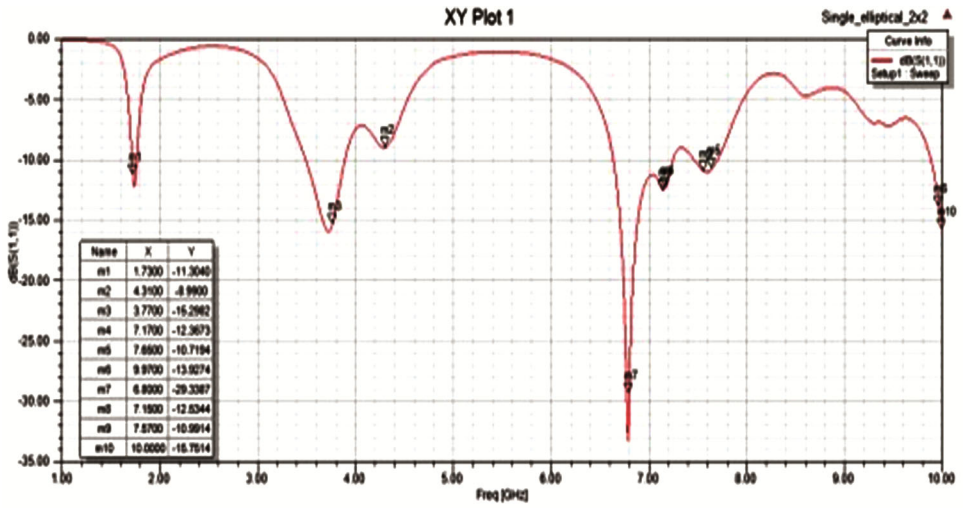

Fig. 20 — Simulated S-parameter of 2x2 MIMO antenna with elliptical DGS for opposite sources are active.

3.7 Simulated results for 2x2 MIMO antenna with elliptical DGS when opposite sources are active and out of phase

3.7.1 Return loss

The return loss of 2x2 MIMO antenna with elliptical DGS when one source is active is shown in Fig. 24. Designed antenna functions at 4 bands i.e., 1.5GHz – 1.80 GHZ, 3.2GHz - 4.6GHz, 6.4GHz – 8.0GHz, 9.0GHz - 10GHz.

3.7.2 2D Radiation patterns

Figure 25 explains the simulated 2D radiation patterns of 2x2 MIMO antenna for opposite sources

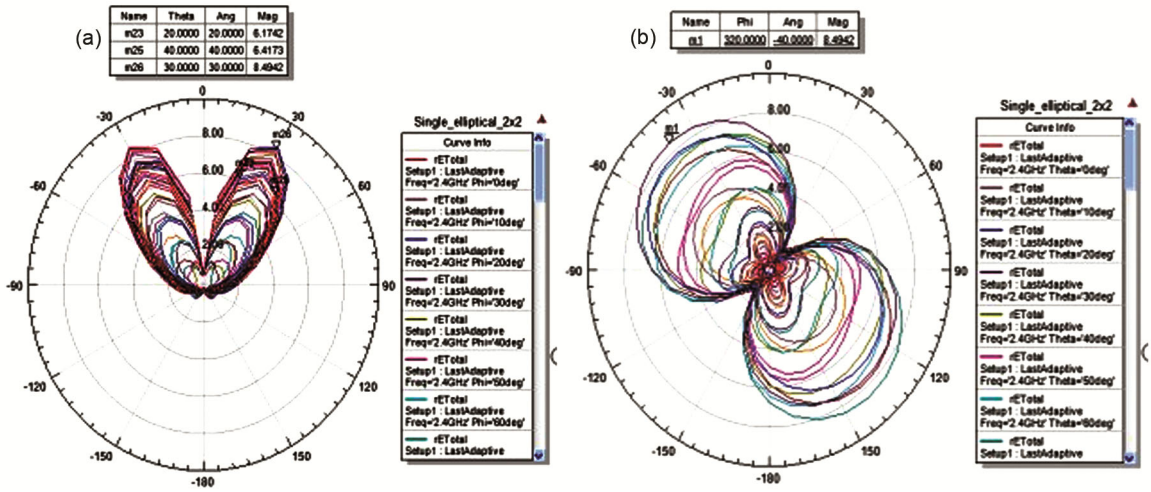

Fig. 21 — Simulated 2D radiation pattern of 2x2 MIMO antenna with elliptical DGS for opposite sources are active: (a) for $\Theta = 360^0$, and (b) for $Pi = 360^0$.

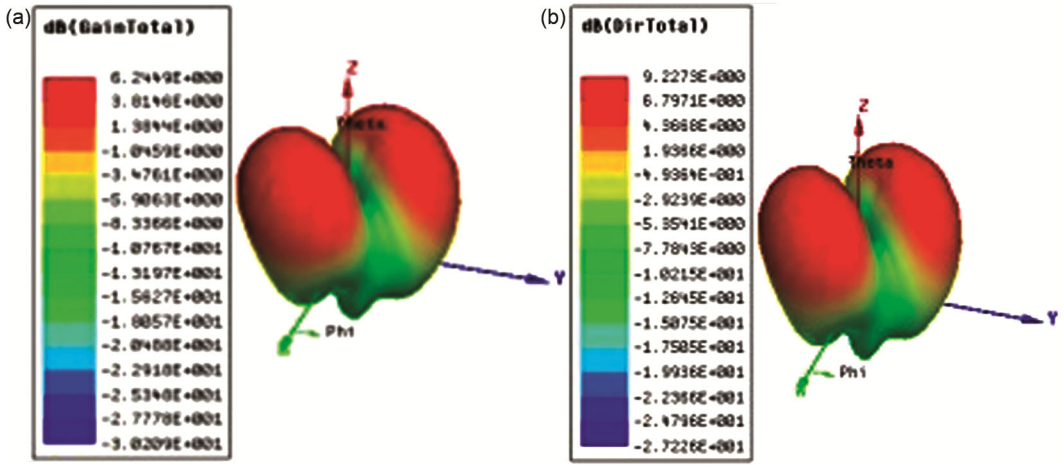

Fig. 22 — Simulated Gain of 2x2 MIMO antenna with elliptical DGS for opposite sources are active (a) Gain, and (b) Directivity.

are active and out of phase. Radiation patterns in principal planes were presented. Fig.25(a), and 25(b) shows the 2D radiation pattern in 2 elevation planes, Θ= 360 X-Z plane, and pi= 360 Y-Z plane. Due to the symmetric shape in the antenna design, radiation pattern was similar for all the combinations of antenna. Radiation patterns similar of monopole were observed for which E_Θ field component represents a dip in end-fire direction for $\Theta = 360^0$, $\Phi = 360^0$. The dip is shifted to 45^0 due to the presence of a symmetric structure. Epi component of $\Phi = 360^0$ is extended towards the end-fire direction. Gain observed from plot as 6.78dBi.

The simulated Gain of 2x2 MIMO antenna with elliptical DGS when opposite sources are out of phase is indicated in Fig. 26. The Gain of the antenna was 7.8dBi. The simulated Directivity of 2x2 MIMO antenna with elliptical DGS when one source is active is denoted in Fig. 26. The directivity of the antenna is 9.9 dBi.

3.7.3 Simulated results

Radiation Efficiency, Radiation Intensity, Radiated Power, and Beam Area of Designed Antenna is displayed in Fig. 27.

3.8 Simulated results for 2x2 MIMO antenna with elliptical DGS when all sources are active and in phase

3.8.1 Return loss

The return loss of 2x2 MIMO antenna with elliptical DGS when one source is active is displayed in Fig. 28. From the plot, it is observed that the antenna functions at 4 bands i.e. 1.5GHz – 1.80 GHZ, 3.2GHz - 4.6GHz, 6.4GHz – 8.0GHz, 9.0GHz - 10GHz.

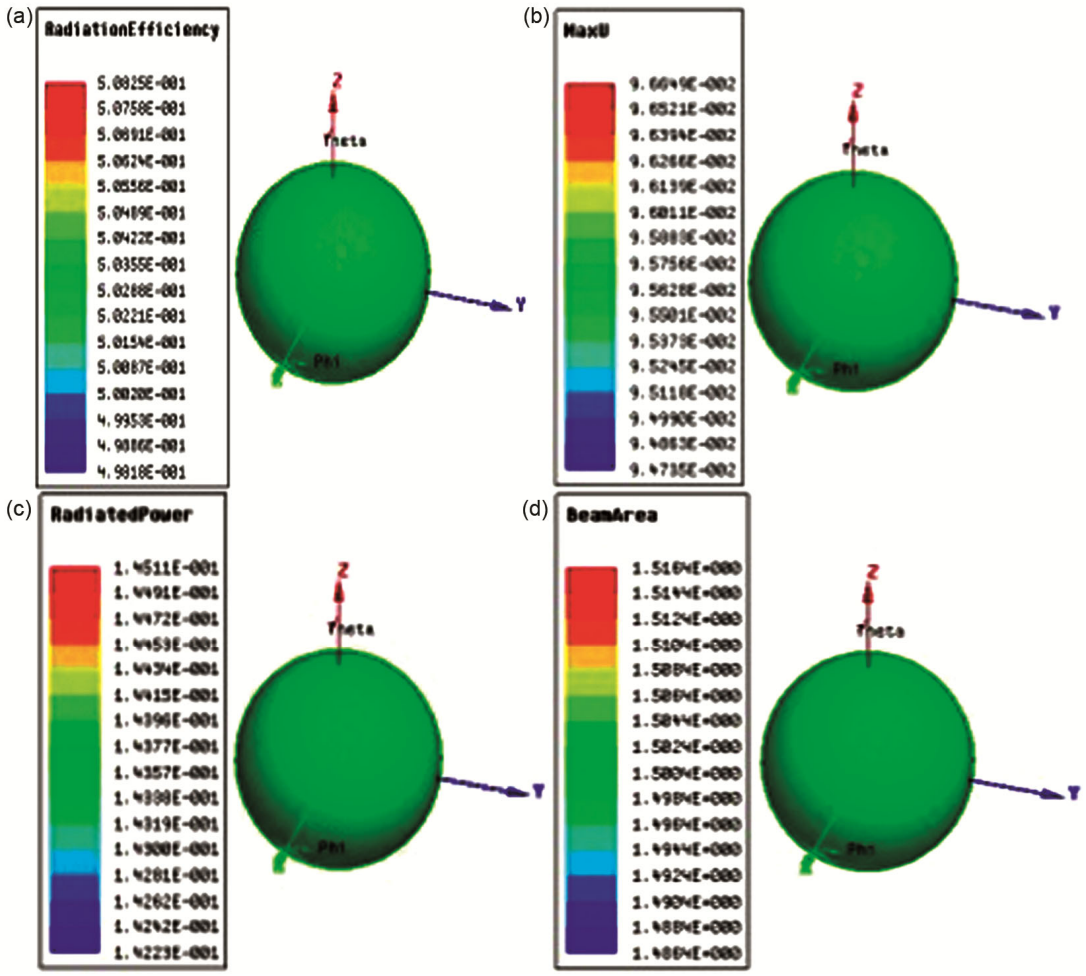

Fig. 23 — Simulated results of 2x2 MIMO antenna with elliptical DGS When opposite sources are active (a) Radiation efficiency, (b) Radiation intensity, (c) Radiated power, and (d) Beam area.

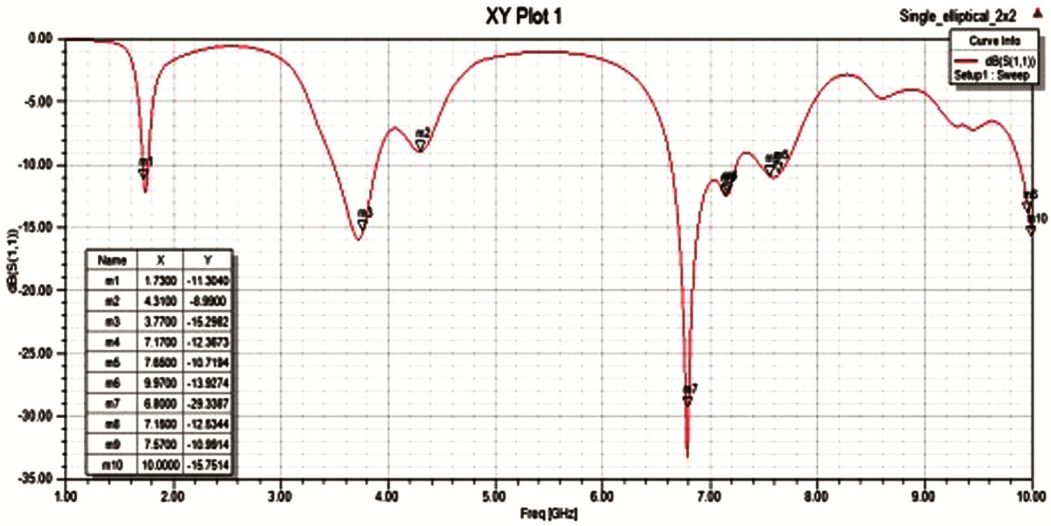

Fig. 24 — Simulated S-parameter of 2x2 MIMO antenna with elliptical DGS for opposite sources are out of phase.

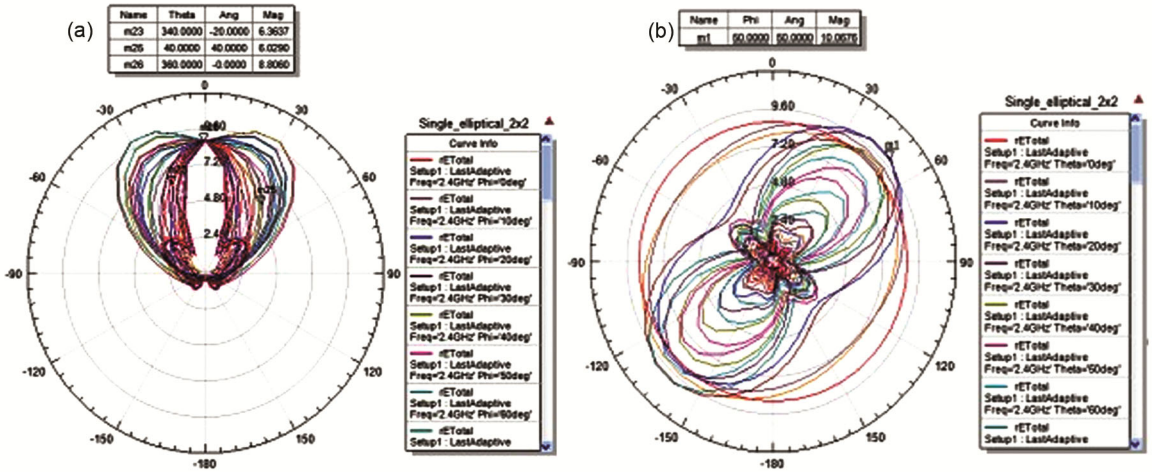

Fig. 25 — Simulated 2D radiation pattern of 2x2 MIMO antenna with elliptical DGS for opposite sources are out of phase: (a) for Θ = 360^0, and (b) for Pi = 360^0.

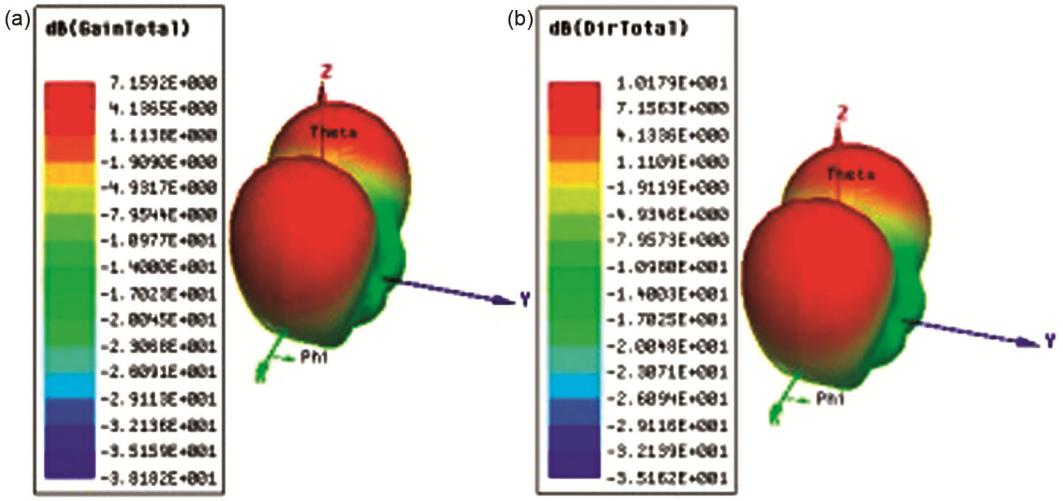

Fig. 26 — Simulated radiation patterns of 2x2 MIMO antenna with elliptical DGS for opposite sources are out of phase (a) Gain, and (b) Directivity.

3.8.2 2D Radiation pattern

Figure 29 indicates the simulated 2D radiation pattern of the 2x2 MIMO antenna for all sources are active. Radiation patterns in principal planes were presented. Fig. 29(a), 29(b) indicates the 2D radiation pattern in 2 elevation planes, Θ= 360 X-Z plane, and pi= 360 Y-Z plane. Radiation patterns similar of monopole were observed for which E_Θ field component represents a dip in end-fire direction for Θ = 360^0, Φ = 360^0. The dip is shifted to 60^0 due to the presence of a symmetric structure. Epi component of Φ = 360^0 is extended towards the broadside direction. Gain observed from plot as 7.1dBi.

The simulated Gain of 2x2 MIMO antenna with elliptical DGS when all source is active is shown in Fig. 30. From the plot, it is noted that the Gain of the antenna is 7.1dBi. The simulated Directivity of 2x2 MIMO antenna with elliptical DGS when one source is active is denoted in Fig. 30. From the plot, it is noted that Directivity of antenna is 9.9dBi.

3.8.3 Simulated results

Radiation Efficiency, Radiation Intensity, Radiated Power, and Beam Area of Designed Antenna is shown in Fig. 31.

3.9 Simulated results for 2x2 MIMO antenna with elliptical DGS when all sources are active and out of phase

3.9.1 Return loss

S parameter of 2x2 MIMO antenna with elliptical DGS when all sources are active and out of phase is shown in Fig. 32. From the plot, it is noted that antenna functions at 4 bands i.e., 1.50GHz – 1.80

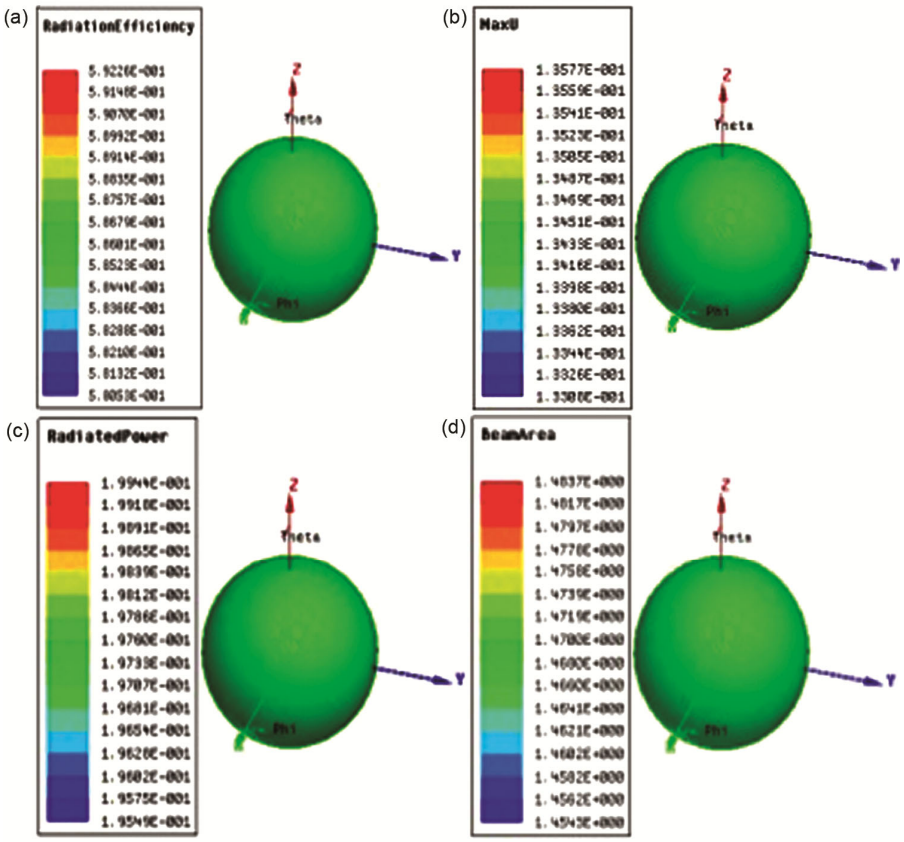

Fig. 27 — Simulated results of 2x2 MIMO antenna with elliptical DGS: When opposite sources are out of phase a) Radiation efficiency, (b) Radiation intensity, (c) Radiated power and (d) Beam area.

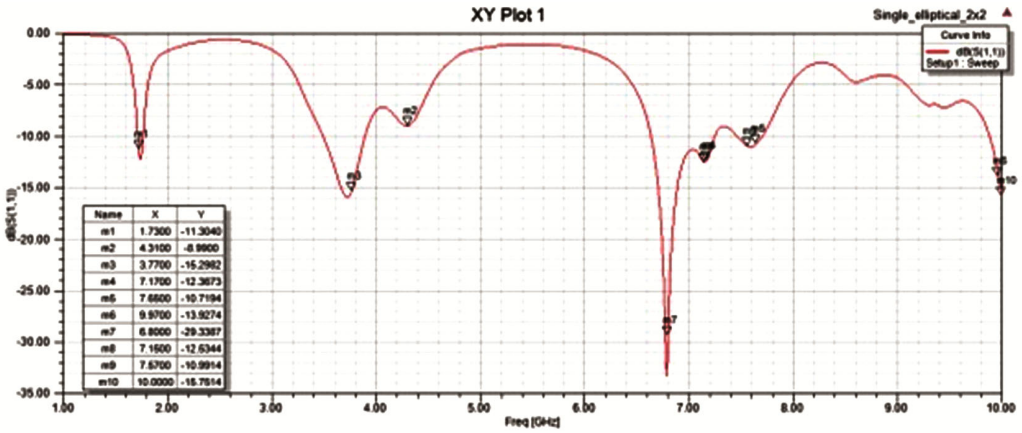

Fig. 28 — Simulated S parameter of 2x2 MIMO antenna with elliptical DGS when all sources are active.

GHZ, 3.2GHz - 4.6GHz, 6.4GHz – 8.0GHz, 9.0GHz - 10GHz.

3.9.2 2D Radiation pattern

Figure 33 shows the simulated 2D radiation pattern of the 2x2 MIMO antenna for all sources are active and out of phase. Radiation patterns in principal planes were presented. Figure 33 (a), 33 (b) shows the 2D radiation pattern in 2 elevation planes, Θ= 360 X-Z plane, and pi= 360 Y-Z plane. Radiation patterns similar of monopole were observed for which E_Θ field component represents a dip in the end-fire direction for $\Theta = 360^0$, $\Phi = 360^0$.

The dip is shifted to 60^0 due to the presence of a symmetric structure. Epi component of $\Phi = 360^0$ is

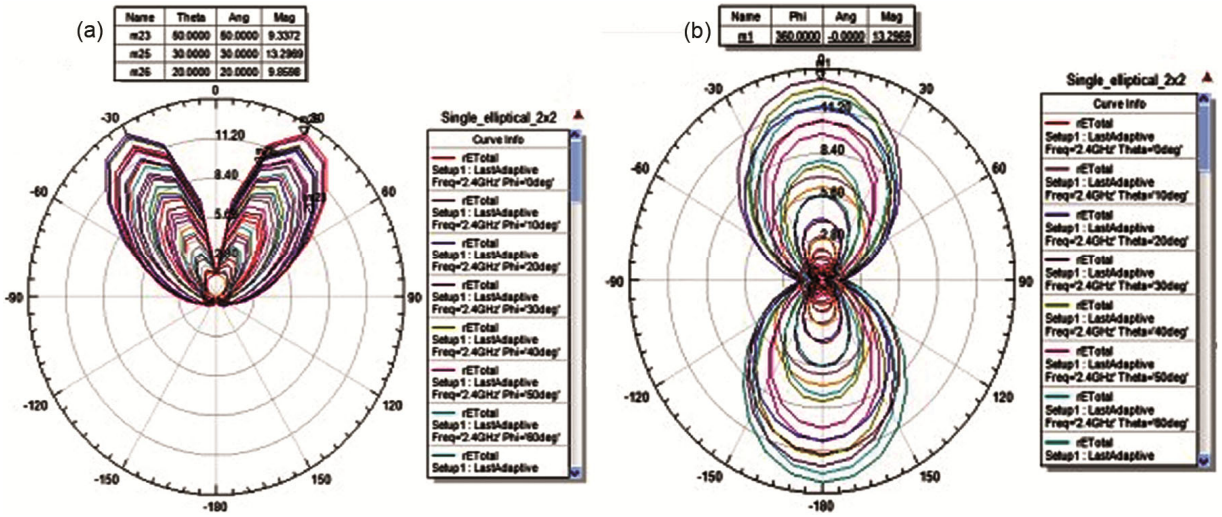

Fig. 29 — Simulated 2D radiation pattern of 2x2 MIMO antenna with elliptical DGS when all sources are active (a) for $\Theta = 360^0$, and (b) for $Pi = 360^0$.

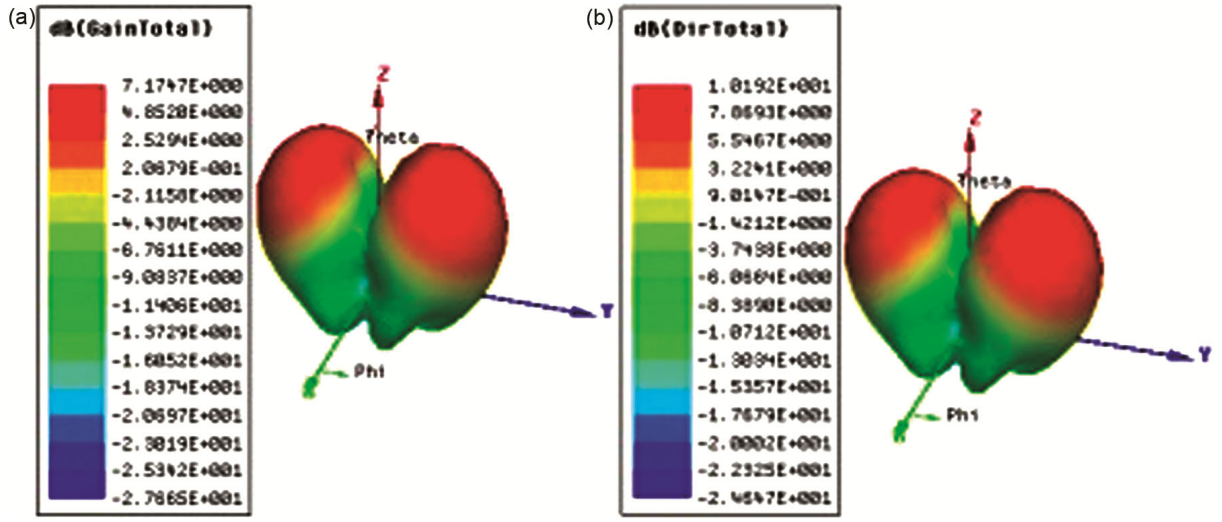

Fig. 30 — Simulated Radiation patterns of 2x2 MIMO antenna with elliptical DGS when all sources are active (a) Gain, and (b) Directivity.

extended towards the end-fire direction. Gain observed from plot as 7.1dBi.

The simulated Gain of 2x2 MIMO antenna with elliptical DGS when all source is active and out of phase is denoted in Fig. 34. it was stated that the Gain of antenna is 7.1dBi. The simulated Directivity of 2x2 MIMO antenna with elliptical DGS when one source is active is shown in Fig. 34. From the plot, it is noted that the Directivity of antenna is 9.8dBi.

3.9.3. Simulated results

Radiation Efficiency, Radiation Intensity, Radiated Power, and Beam Area of Designed Antenna is shown in Fig. 35.

3.9.4 Envelope correlation coefficient (ECC)

Represents the correlation between antennas. It is calculated from the S-parameter or radiation pattern. Here ECC was calculated from the S-parameter. Normally ECC should be <0.5 for MIMO antenna. From the simulated plot, ECC is less than 0.2 for all operating bands, that indicates that the designed antenna is appropriate for 5G with enhanced isolation. The return loss of 2x2 MIMO antenna with elliptical DGS when one source is active is displayed in Fig. 36. From the plot, it is observed that the antenna functions at 4 bands i.e. 1.5GHz – 1.80 GHZ, 3.2GHz - 4.6GHz, 6.4GHz – 8.0GHz, 9.0GHz - 10GHz

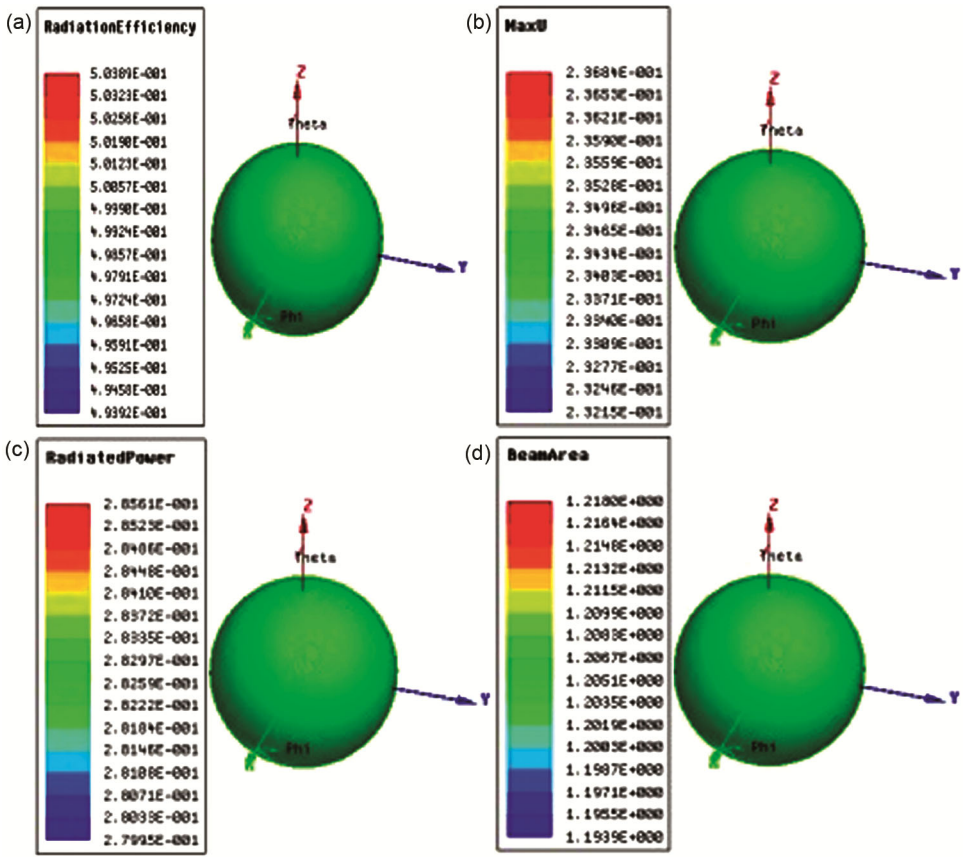

Fig. 31 — Simulated results of 2x2 MIMO antenna with elliptical DGS: When all sources are active a) Radiation efficiency, (b) Radiation intensity, (c) Radiated power, and (d) Beam area.

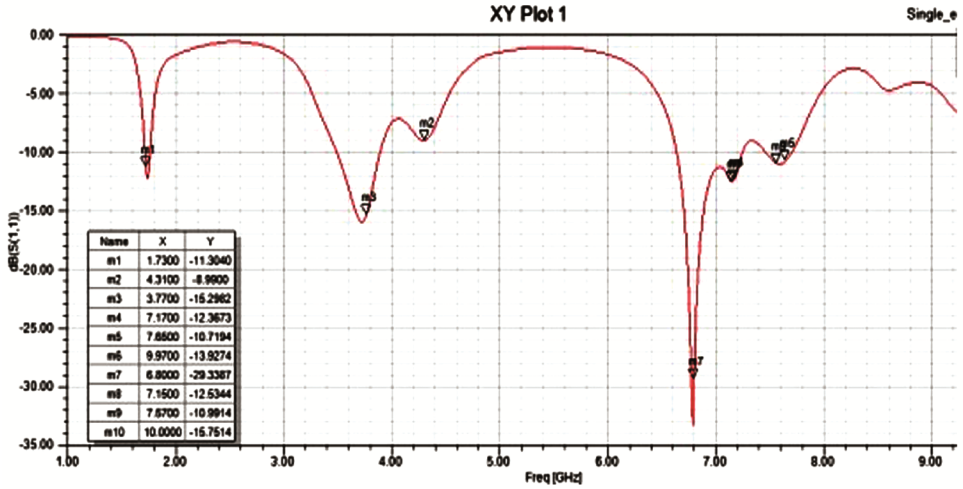

Fig. 32 — Simulated S parameter of 2x2 MIMO antenna with elliptical DGS when sources are out of phase.

Table 1 gives the summary results for different antenna combinations in terms of Active and phase shifts. In all the combinations, the antenna operated at approximately similar bands but enhanced in gain. For 2x1 MIMO antenna, when only one antenna is made active, achieves a gain of 1.20 dBi. For 2x1 MIMO antenna, when Two Sources are Active and in-phase, achieves a gain of 2.85 dBi. For 2x1 MIMO antenna, when Two Sources are Active and out of phase, achieves a gain of 5.41 dBi. For 2x2 MIMO antenna, when One Source is Active achieves a gain of 7.07 dBi. For 2x2 MIMO antenna, when Opposite

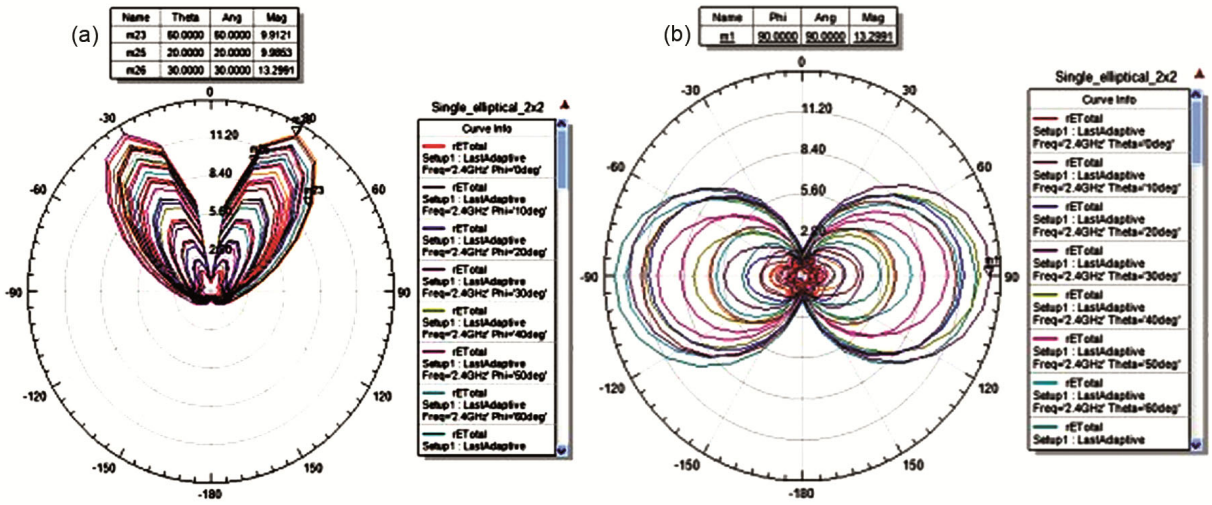

Fig. 33 — Simulated 2D radiation pattern of 2x2 MIMO antenna with elliptical DGS when sources are out of phase (a) for $\Theta = 360^0$, and (b) for $Pi = 360^0$.

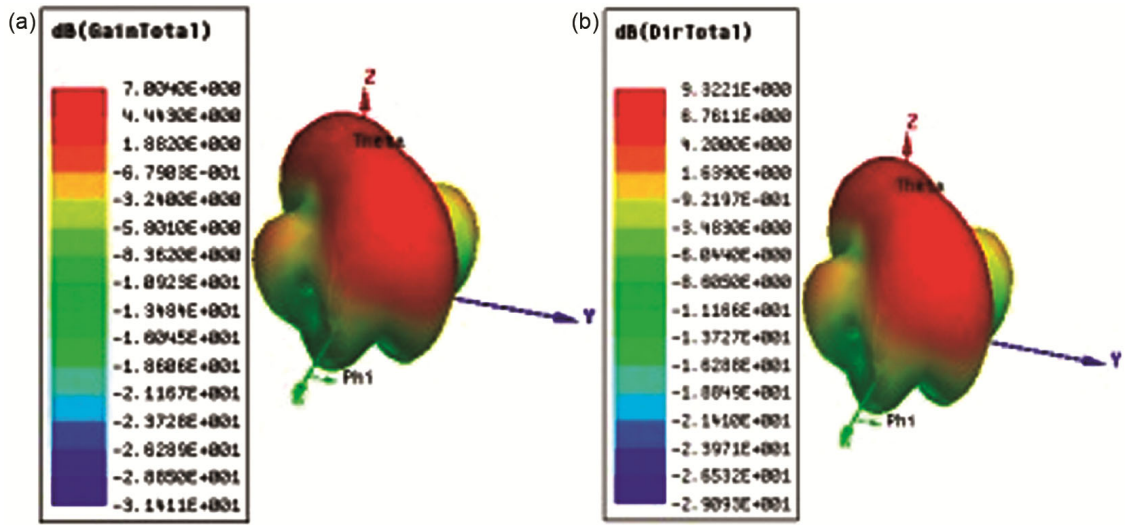

Fig. 34 — Simulated Gain of 2x2 MIMO antenna with elliptical DGS when sources are out of phase (a) Gain, and (b) Directivity.

Sources are Active and in phase achieves a gain of 7.15 dBi. For 2x2 MIMO antenna, when Opposite Sources are Active and out of phase, achieved a gain of 7.17 dBi. For 2x2 MIMO antenna, when All Sources are Active, and in-phase achieves a gain of 7.29 dBi. For 2x2 MIMO antenna, when All Sources are Active and out of phase, achieves a gain of 7.80dBi.

3.10 Performance analysis of proposed antenna with other existing antenna designs

Simulated results of the proposed antenna are compared with the existing implemented designs[1-7,12,18] in terms of patch geometry, feeding techniques, operating frequency bands, number of frequency bands, ECC & Gain of the antennas.

Simulated results for proposed antenna are compared with existing implemented designs[1-7,12,18] in terms of patch geometry, feeding techniques, operating bands, number of bands, ECC & Gain of antennas. A summary of those results was tabulated in Table 2. Kin-Lu Wong et al. designed an 8-port angular ring slotted patch with 16 shorting pins connected to a circular grounded MIMO antenna for mobiles[1]. From circular patches, 8 angular ring patches are made with the help of 8 open slots. Each angular ring patch is fed with a probe feed technique

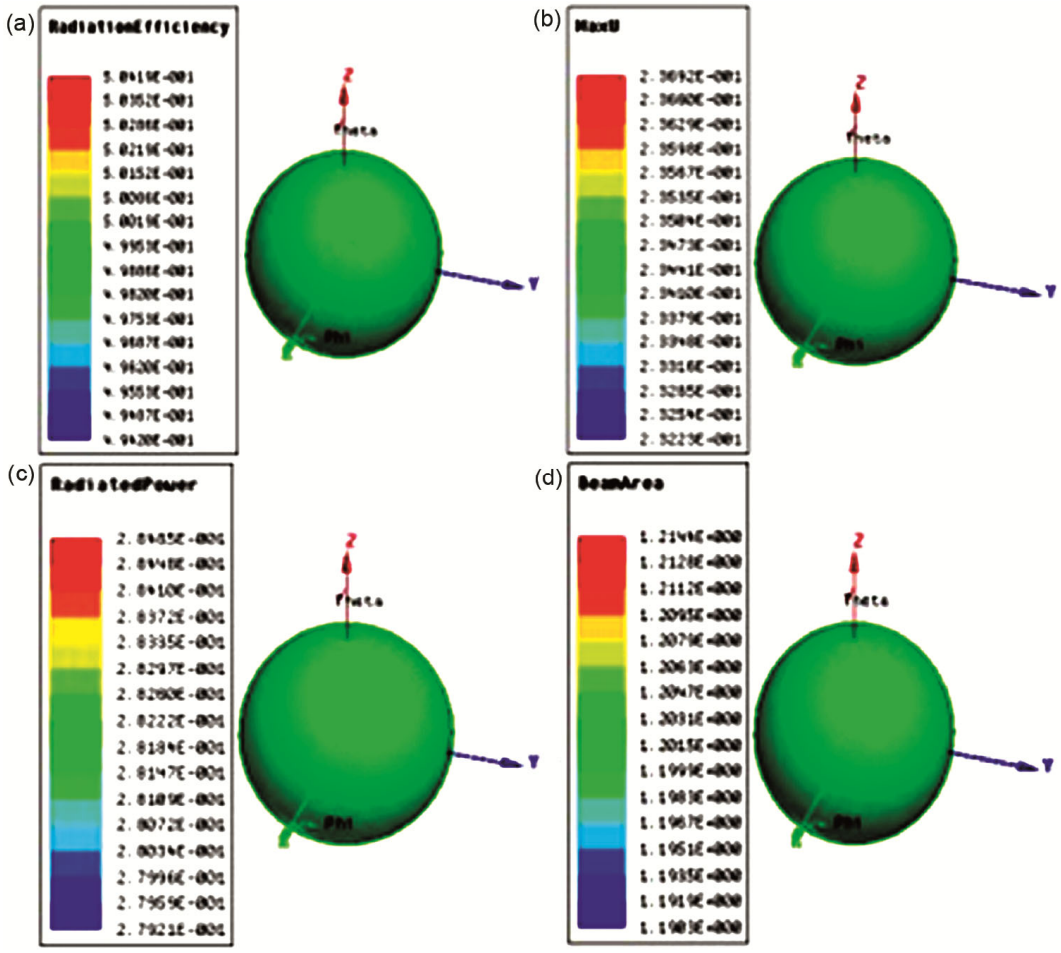

Fig. 35 — Simulated results of 2x2 MIMO antenna with elliptical DGS: When sources are out of phase a) Radiation efficiency, (b) Radiation intensity, (c) Radiated power, and (d) Beam area.

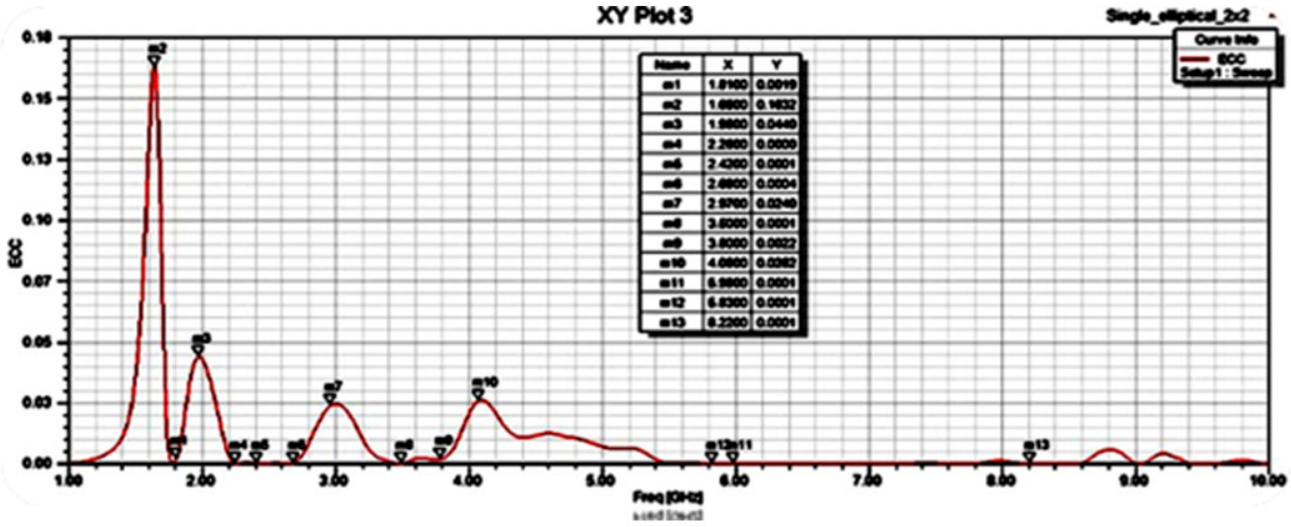

Fig. 36 — Simulated ECC of 2x2 MIMO antenna with elliptical DGS when sources are out of phase.

Table1 — Comparison of antenna parameters of 2x1 and 2x2 MIMO antennas with different operating conditions of sources.

Antenna Type	Antenna Combinations	No. of Active sources	The phase shift between Antennas	Operating Frequency bands	Gain (dBi)
2x1 MIMO Antenna	One Source is Active	1	One Source	1.5 GHz – 1.80 GHZ, 3.20 GHz - 4.6GHz, 6.4GHz – 8.0GHz, 9.20GHz – 10GHz.	1.20
	Two Sources are Active and in-phase	2	In phase	1.5 GHz – 1.80 GHZ, 3.20 GHz - 4.6GHz, 6.4GHz – 8.0GHz, 9.20GHz – 10GHz.	2.85
	Two Sources are Active and out of phase	2	Out of phase	1.5 GHz – 1.80 GHZ, 3.2GHz - 4.6GHz, 6.4GHz – 8.0GHz, 9.20GHz – 10GHz.	5.41
2x2 MIMO Antenna	One Source is Active	1	One Source	1.5 GHz – 1.80 GHZ, 3.2GHz - 4.6GHz, 6.4GHz – 8.0GHz, 9.20GHz – 10GHz.	7.07
	Opposite Sources are Active and in-phase	2	In phase	1.5 GHz – 1.80 GHZ, 3.2GHz - 4.6GHz, 6.4GHz – 8.0GHz, 9.20GHz – 10GHz.	7.15
	Opposite Sources are Active and out of phase	2	Out of phase	1.5 GHz – 1.80 GHZ, 3.2GHz - 4.6GHz, 6.4GHz – 8.0GHz, 9.20GHz – 10GHz.	7.17
	All Sources are Active and in-phase	4	In phase	1.5 GHz – 1.80 GHZ, 3.2GHz - 4.6GHz, 6.4GHz – 8.0GHz, 9.20GHz – 10GHz.	7.29
	All Sources are Active and out of phase	4	Out of phase	1.5 GHz – 1.80 GHZ, 3.2GHz - 4.6GHz, 6.4GHz – 8.0GHz, 9.20GHz – 10GHz.	7.80

Table 2 — Comparison of the proposed antenna with previous existing antennas.

Patch Shape	Feeding Technique	Operating Frequency Bands (GHz)	No. of Frequency Bands	ECC	Antenna Gain (dBi)
Sectored Ring[1]	Coaxial Probe Feed	5.925-7.125 GHz	1	ECC<0.8	1.2-4.1
Circular Ring[2]	Microstrip line	5.82- 5.94 GHz	1	ECC<0.1	7.68
Elliptical patch antenna[3]	Coplanar waveguide Feed	24.25-27.5 GHz	1	ECC<0.1	2.2-5.3
Pyramid patch antenna[4]	Coaxial Probe Feed	2.9- 11 GHz	1	ECC <0.75	8.3
Alford Loop antenna[5]	Microstrip line	2.4- 2.5 GHz, 5.1-5.9 GHz	2	ECC< -7.2	3.2
Y- shaped antenna[6]	Microstrip line	3.3- 4.2 GHz	1	ECC< 0.5	4
Square Patch antenna[7]	Microstrip line	5.7- 5.8 GHz	2	ECC< 0.5	7
Inverted F Antenna[12]	Coaxial Probe Feed	1.73GHz, 2.29- 2.68GHz	2	ECC<0.15	2.85
Orthogonal monopole antenna [18]	Microstrip line	2.20- 3.15 GHz, 5.24-5.83 GHz	2	ECC<0.5	3.52, 4.24
Proposed Antenna	Microstrip line	2.40 -2.60GHz, 3.20-3.60 GHz, 4.80- 5.20GHz, 7.20-7.80 GHz, 8.20- 8.40GHz, 9.60 -10.0GHz.	6	ECC<0.1	7.80

to form 8 ports. Below the feed point, towards the center 2 shorting pins were used to short patch and ground to suppress standing waves and hence improve the isolation between patches. So low value of ECC < 0.1 is achieved for MIMO operation. The designed antenna operated at 5.9-7.2 GHz in the 6GHz band which can be used for future 6G mobile communications and IoT but the designed antenna operated at only one band. Md. Abu Sufian et al. designed Four square-shaped patches, placed in an orthogonal manner on the substrate[2]. Circular-shaped parasites were incorporated between 4 square patches to reduce common coupling effect between nearby antenna elements. Designed antenna operated at 5.82- 5.94 GHz band with 7.68dBi gain. Ground plane is defected with four arm fan shaped defects to reduce common coupling effect involving four adjacent square patches. The proposed antenna can be implemented for vehicles for intercommunication. However, the designed antenna can be operated at only one band.

Sanjukta Nej et al. designed Ten elements asymmetric U-shaped patch antenna on Fr4 substrate to operate in the N258 band[3]. An elliptical-shaped slot is made at each patch area and an asymmetric U-shaped patch is inserted with the help of a coplanar waveguide. Here 10 ports were used to connect 10 asymmetric U patches. Defected ground with an elliptical shape is done to reduce the common coupling effect connecting antennas. Selecting the shape and position of DGS plays an important role in reducing surface currents and in turn minimizes mutual coupling effect and improves isolation. The designed antenna is operated at only one frequency band. Praveen Kumar et al. designed a 6-port symmetrical pyramid antenna using a novel defected ground plane with better isolation[4]. Rectangular-shaped defects were made on the ground bottom at each pyramid patch. This slot creates a disturbance in the current distribution and improves isolation. Two vertical branches and one horizontal branch were made on the ground to separate six grounds below six patches. Decoupling structure made on the ground creates reverse currents in opposite direction and minimize mutual coupling between elements. However, the designed antenna can be operated at only one band. Peng Fei Hu et al. designed A miniaturized dual-band loop antenna to function at 2.4 GHz & 5 GHz WIFI bands[5]. The circular loop antenna is fed with four strips connected to the center using a coaxial probe feed technique. Two loop patches are arranged compactly on a common substrate to operate at the 2.4GHz band and 5GHz band independently. Normal loop is used for the 2.4GHz band and the Alford loop is used for the 5GHz band. However, the designed antenna can be operated at only two frequency bands.

Kin-Lu Wong et al. designed Three port Y-shaped monopolar MIMO antenna, operating at 3.3-4.2 GHz[6]. Three shorting strips were used at the three edges of Y and one strip on the center of Y was made to form three monopolar patches. A circular-shaped ground plate is used in the design with a coaxial probe feed technique. The designed antenna is used for 5G communication. The measured & simulated ECC for the intended antenna is < 0.1 in the operated bands, which indicates better radiation characteristics of MIMO operation. However, the designed antenna can be operated at only one frequency band. Jogesh Dash, and Debdep Sarkar designed two closely spaced patches with an inverted L-shaped structure connected at one end of each patch from top to bottom with rectangular DGS for 5G applications[14]. Two patches are fed with a coaxial probe feeding technique. Inverted L shaped arrangements were attached to patches to create asymmetry to decrease mutual coupling between patches and improve isolation. However, the designed antenna can be operated at only two frequency bands. Two-element inverted F shaped MIMO antenna is designed for WLAN purposes[15]. Two IFAs on top act as antenna 1,2 and the bottom layer with two angular slots acts as antenna 3,4. The two angular slots on ground improve the isolation between elements. The novelty in this approach is converting the DGS structure on the ground to an antenna. However, the designed antenna can be operated at only two frequency bands. Kaikai Song designed dual-band printed monopole MIMO antenna to LTE and WLAN functions. However, the designed antenna can be operated at only two frequency bands[16].

In the proposed design, a modified square slot was made at the center of the patch, and eighteen rectangular slots around the borders of the patch in the form of a modified Sierpinski carpet fractal structure. Multiband and Miniaturization characteristics are obtained with a novel modified fractal structure. Miniaturization and multiband characteristics are obtained with the help of a novel modified fractal structure. Then two such antennas were combined to form a 2x1 MIMO antenna. Further 2x2 MIMO antenna is designed with 4 elements. The purported 2x2 MIMO antenna consists of four novel modified Sierpinski carpet-shaped antenna elements. Four antenna elements were closely separated with $\lambda/2$. Novel defected ground structures with ellipses were made to achieve high isolation within 4-elements of MIMO antenna. The designed antenna is simulated for different combinations of Active sources and phase shifts. Designed antenna is operated for Nine 5G NR bands including N3 (1.710- 1.785) GHz for DCS, N24 (1.626- 1.66)GHz, N48 (3.55- 3.70) GHz, N66 (1.710- 1.780) GHz for Extended AWS, N70 (1.1695- 1.710) GHz for supplementary AWS, N77 (3.30- 4.2) GHz, N78 (3.30- 3.8) GHz, N80 (1.710- 1.785) GHz for DCS, N99 (1.626- 1.660) GHz for upper L-band US and N104 (6.425- 7.125) GHz and 3 N IoT bands (B3, B4, B70), 3.5 GHz WIMAX band. The novel design structure enhanced multiband characteristics and improved miniaturization represents that proposed antenna will be an efficient candidate for future wireless communication systems including IoT.

4 Conclusion

In this paper, a multi-band 2x2 MIMO antenna was designed for future mobile communications. Patch consisting of a modified square slot at the center and eighteen slots around the center slot. Different designs like single, 2x1, and 2x2 MIMO antennas were designed and various antenna parameters were measured. The dimensions of the proposed antenna are 45x45x1.6mm^3. Designed antenna is operated for Nine 5G NR bands including GPS, N3 (1.710- 1.785) GHz for DCS, N24(1.626- 1.660)GHz, N48 (3.55- 3.70) GHz, N66 (1.710- 1.780) GHz for Extended AWS, N70 (1.1695- 1.710) GHz for supplementary AWS, N77 (3.3- 4.2) GHz, N78 (3.3- 3.8) GHz, N80 (1.710- 1.785) GHz for DCS, N99 (1.626- 1.660) GHz for upper L-band US and N104 (6.425- 7.125) GHz and 3 N IoT bands (B3, B4, B70), 3.5 GHz WIMAX band. The ECC value of the proposed antenna is less than 0.1 for all operating bands, indicating that the designed MIMO antenna is appropriate for 5G and future mobile terminals with enhanced isolation.

References

1 Kin-Lu Wong, Hui-Chih Kao, Wei-Yu Li, *IEEE Access,* 11 (2023) 18.

2 Md. Abu Sufian, Niamat Hussain, Anees Abbas, Jaemin Lee, Seong Gyoon Park, Nam Kim, *IEEE Access*, 10 (2022) 56388.

3 Sanjukta Nej, Anumoy Ghosh, Sarosh Ahmad, Jayendra Kumar, Adnan Ghaffar, Mousa I. Hussein, IEEE Access, 10 (2022) 125086.

4 Praveen Kumar, Sameena Pathan, Om Prakash Kumar, Shweta Vincent, Yashwanth Nanjappa, Pradeep Kumar, Pranav Shetty, Tanweer Ali, *IEEE Access*, 10 (2022) 112964.

5 Peng Fei Hu, Kwok Wa Leung, Yong Mei Pan, and Shao Yong Zheng, *IEEE T AP*, 69 (2021) 5345.

6 Kin-Lu Wong, Hsuan-Jui Chang, Jian-Zhong Chen, Kuan-Ying Wang, *IEEE AWPL*, 19 (2020) 393.

7 Jogesh Chandra Dash and Debdeep Sarkar, *IEEE Access,* 9 (2021) 156222.

8 JingYa Deng, JinYong Li, Luyu Zhao and LiXin Guo, *IEEE AWPL*, 16 (2017) 2270.

9 Wen Wang, Yongle Wu, Weimin Wang, and Yuhao Yang, *IEEE T Circuits and Systems II: Express Briefs,* 68 (2021) 1867.

10 Zhuo-Lin Zhao, Cheng-Zhu Du, Kai-Jia Li, Gao-Ya Jin, Wei-Qing Zheng, Fu-Hui Yang Shanghai, *2020(ICMMT)*, China, (2020).

11 Zhipeng Zhao, Feng Liu, Jian Ren, and Yingzeng Yin, *2019 Photonics & Electromagnetics Research Symposium - Fall (PIERS - Fall)*, Xiamen, China, (2019) 2987.

12 Rifaqat Hussain, Muhammad Umar Khan, and Mohammad S. Sharawi, *IEEE AWPL*, 17 (2018) 142.

13 Jian Ren, Wei Hu, Member, IEEE, Ying Zeng Yin, and Rong Fan*, IEEE AWPL*, 13 (2014) 1517.

14 Kin-Lu Wong, Guan-Lin Yan, *IEEE Access*, 10 (2022) 893.

15 Chao Wang; Hanyang Wang; Pengfei Wu; Meng Hou, *IEEE T AP*, 70 (2022) 6514.

16 Soumik Dey, Sukomal Dey and Shiban K. Koul, *IEEE Access,* 9 (2021) 162820.

17 S. Ashok Kumar and T. Shanmuganantham, D. Dileepan, *AEJ,* 56 (2017) 231.

18 Kaikai Song, Guizhen Lu, Fanruiqi Zeng, *IEEE Access*, 15 (2015) 5.

19 Srinivasan Ashok Kumar and Thangavelu Shanmuganantham, *JCSC*, 24(2015) 1.

20 T. Shanmuganantham, S. Ashok Kumar, *AEU: I J EC*, 68 (2014) 158.